Quantifying Female Subject-specific Knee-thigh-hip Responses in Frontal Impact Scenarios

Randolff L. Carpenter, Parker R. Berthelson, John-Paul Donlon, Jason L. Forman

Abstract Four female post-mortem human subjects (PMHS) with varying anthropometry were tested under bilateral knee impact conditions using a pneumatically driven ram. Ten tests were performed on each PMHS, varying the velocity at impact and the coupled mass of the knee-thigh-hip (KTH) system. Test conditions included whole body (WB), removal of thigh flesh (TFR), the addition of implantable femur load cells (TFR+LC), and the removal of the torso (ToR). By removing these masses coupled to the KTH complex, individual component contributions were then analysed. Using the component masses that were obtained during autopsy and the accelerometer and force data recorded during testing, a one-dimensional subject-specific lumped-parameter model (LPM) was developed for KTH. The average force transfer predicted by the completed LPMs was 70.6±1.7% from the knee to the mid-femur and 57.0±3.0% from the knee to the hip. Finally, across all subject conditions, the percentage of force that transferred from the knee generally decreased with increasing impact velocity. Development of the LPMs provides a crucial first step in beginning to characterize female KTH injury risk in frontal collisions, to eventually translate KTH injury risk functions to female anthropomorphic test devices and human body models.

Keywords Female, Frontal Impacts, Knee-Thigh-Hip, Lumped-Parameter Modelling, PMHS.

I. INTRODUCTION

Knee-thigh-hip (KTH) injuries account for 25% of the life-years lost due to injury in frontal collisions, with injuries to the hip comprising approximately 65% of that value [1]. KTH loading is primarily caused by the occupant's interaction with the lower instrument panel during a frontal collision. The force is transferred through the knee, along the femur, and to the hip. Injuries can occur at any point along the load path; however, the force transferred to the hip comprises a fraction of the initially applied force at the knee - the force applied to the knee is expended by the acceleration of the increasingly recruited mass along the KTH load path. The knee-to-hip force transfer thus depends on the structural and material factors of the KTH complex—for example, the mass distribution of the flesh or the coupling of the flesh to the bone. As the force-tolerance varies among the various anatomical locations along the KTH load path, the nature of the force transfer along the KTH can affect not only the location of injury but also the risk of injury dependent on both the magnitude and duration of the applied load.

To measure the force transfer characteristics of the KTH complex, a combined experimental and modelling approach is required. Rupp and co-authors developed a one-dimensional lumped parameter model (LPM) for mid-sized male post-mortem human subjects (PMHSs) using data from padded knee impact tests with the PMHS seated upright in a free back condition [2]. Through approximately 250 tests on five PMHSs, varying both the velocity at impact and the amount of mass coupled to KTH, differences in loading and kinematics were related to mass, spring, and damper analogues [2]. From here, it was estimated that the hip force comprised 53.7±0.9% of the initially applied force at the knee. While this represented a substantial advancement in understanding KTH force transfer, the representativeness of the findings for a broader population was unproven. In particular, the effect of sex on KTH force transfer remains unexplored, although sex-correlated physiological differences may contribute to higher risk of KTH injury to females in frontal crashes [3,4].

This study aimed to quantify the response of small females to frontal KTH loading. To achieve this, a multipart analysis was performed. Four female PMHSs were impacted bilaterally at the knees by a padded ram. Ten tests were performed hierarchically on each PMHS, varying the velocities at impact and the mass coupled to KTH, adapting the test procedure from the methods and findings of [2]. The experimental results were then used to create subject-specific LPMs for female KTH. With the completed models, it was then possible to analyse segment

contributions and the resulting force transfer along KTH.

II. METHODS

Experimental Methodology

To simulate a frontal KTH impact, seated PMHSs were struck in the knees by a ram coupled to a pneumatically driven linear actuator and servo-hydraulically controlled with active feedback (DSD, Linz, Austria) (Fig. 1.). Each knee was struck by an impacting assembly consisting of a six-axis load cell (Model 3868TF, Robert A. Denton, Inc.) covered by a 25 mm-thick pad of 50-durometer (Shore OO scale) Sorbothane padding on top of a 25 mm-thick pad of 70-durometer (Shore OO scale) Sorbothane (Sorbothane Inc., Kent, Ohio) [2]. The seat and footpan were lined with a low-friction material and mounted on six-axis load cells (Model M3255, Sunrise Instruments LLC).

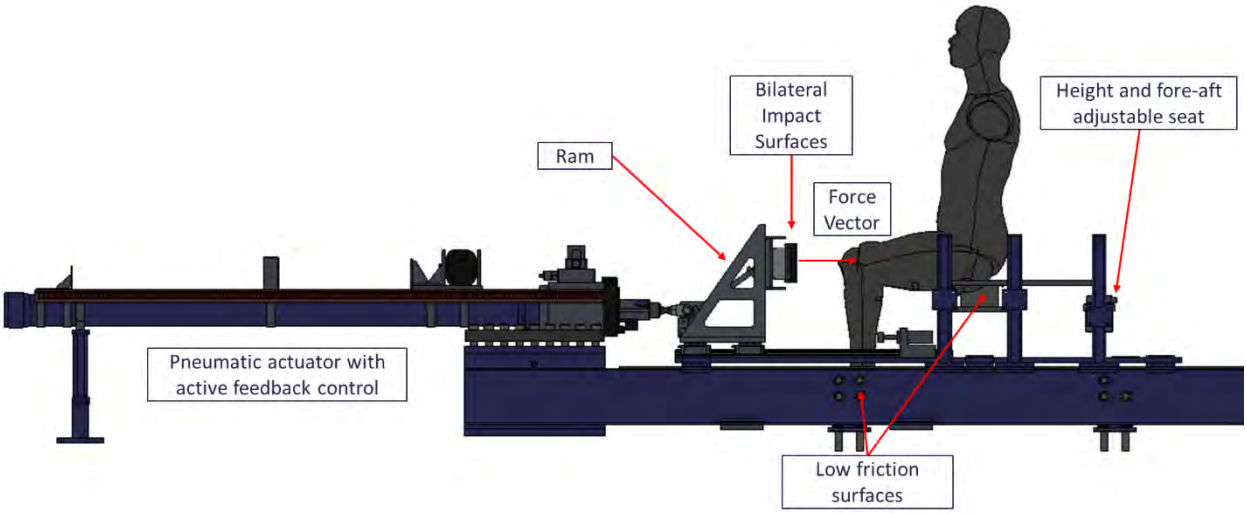

Fig. 1. Overview of test fixture. A pneumatic actuator linearly accelerated a ram with padded impact surfaces into the PMHSs' knees while the PMHSs sat on a low-friction seat and foot support.

Each PMHS was tested at velocities of 2.5, 3.5, 4.9, and 7.2 m/s. The ram accelerated to the target velocity before striking the PMHS, maintained a constant velocity during the impact, and then decelerated before the legs of the PMHS struck the seat. The 3.5 m/s and 4.9 m/s were selected based on previous KTH impact velocities derived from FMVSS 208 and NCAP data [2]. The 2.5 m/s and 7.2 m/s impact velocities were chosen to assess female KTH response across a wider range of impact frequencies.

Tests for each PMHS followed the hierarchical procedure and used the naming conventions of [2] (Table 1). Three tests were performed with the intact PMHS (*whole body* or WB condition; Fig. A1) at velocities of 2.5, 3.5, and 4.9 m/s. After the WB testing, the flesh was removed from each thigh (*thigh flesh removed* or TFR condition; Fig. A2) and the PMHS was tested once at 3.5 m/s. After this, a portion of each femoral shaft was removed and replaced with an implantable six-axis load cell (*thigh flesh removed plus load cell* or TFR+LC condition; Fig. A3). Three tests were performed in the TFR+LC condition at velocities of 2.5, 3.5, and 4.9 m/s. Finally, the torso was removed from the PMHS (*torso removed* or ToR condition; Fig. A4), and three tests were performed at velocities of 3.5, 4.9, and 7.2 m/s.

TABLE I
PER-PMHS TEST MATRIX

Test Number	PMHS Condition	Target Impact Velocity (m/s)
1	Whole Body (WB)	2.5
2	Whole Body (WB)	3.5
3	Whole Body (WB)	4.9
4	Thigh Flesh Removed (TFR)	3.5
5	Thigh Flesh Removed Plus Load Cell (TFR+LC)	2.5
6	Thigh Flesh Removed Plus Load Cell (TFR+LC)	3.5
7	Thigh Flesh Removed Plus Load Cell (TFR+LC)	4.9
8	Torso Removed (ToR)	3.5
9	Torso Removed (ToR)	4.9
10	Torso Removed (ToR)	7.2

Before the WB tests, the PMHSs' forearms were removed at the elbow to prevent the upper limbs from interacting with instrumentation. Mounts to install inertial measurement sensors and motion-tracking markers were attached to each femur (by a hose clamp about the femoral shaft), the pelvis (by screws in the posterior superior iliac spines), and the L2 vertebra (by screws in the laminae) (Fig. B1 and B2). Mounts for motion-tracking markers were also attached to the T1, T8, and L2 vertebrae. The positions of instrumentation relative to anatomical landmarks were measured through computed tomography (CT) imaging (Fig. B3).

Before the TFR tests, the flesh between the gluteal fold and the popliteal fossa was removed from each thigh, leaving the femoral shafts clear of soft tissue (Fig. C1). The mass of removed thigh flesh was measured for use in developing the LPM.

Before the TFR+LC tests, a load cell was implanted at the mid-shaft of each femur (Fig. D1). Bone sections of approximately 10 cm in length were removed from each femur. The segmented ends were potted within aluminium cups with reinforced fiberglass filler (Bondo® Hair). Pins were passed through bicortical holes in the femur and into the cups to align and fix the bone. The positions and orientations of the potting cups relative to anatomical landmarks were then confirmed through CT imaging (Figure D2).

Before the ToR tests, the organ block was removed from the torso, and the torso was sectioned at the level of the L3 vertebra. A rod was inserted in the L3 vertebral body to facilitate positioning of the PMHSs.

Instrument data were collected with Slice Pro, a data acquisition system (Diversified Technical Systems Inc.) that acquired data at 10,000 samples/sec. Triaxial accelerations and angular rates were measured at the femurs, pelvis, and L2 (6DX Pro, DTS Inc.). Six-axis loads were measured in the femurs (Model 6166J, Robert A. Denton, Inc.). Six-degree-of-freedom translations and rotations were measured at the femurs, pelvis, and the T1, T8, and L2 vertebrae. All accelerations, angular velocities, and loads were filtered at CFC 60 (SAE J211, 2014) based on frequency analysis of the signals. The accelerations of anatomic reference frames on the pelvis, femurs, and L2 were calculated using CT imaging and motion tracking [5]. Tracked locations included the proximal and distal shaft of the femur, hip joint centre of the pelvis, and centre of L2. Values are reported in the primary loading direction oriented anteriorly-to-posteriorly. Response curves are reported as the average PMHS response ± one standard deviation (SD).

The loads measured at the ram, seat, and footpan were inertially compensated using the masses of the assemblies and the measured accelerations of the assemblies. Contact timing was determined as the time when the applied knee force was last below one percent of the peak force value. Knee loading curves were further analysed to determine the loading rate, loading duration, peak force, and time to peak force as a function of anthropometry and test conditions, with definitions for each measurement kept consistent with [2].

PMHS

Four female PMHSs were used in this study. A full-body CT scan and dual-energy X-ray absorptiometry (DXA) were used to confirm the absence of implants and injuries in the lower extremities and to analyse bone quality by obtaining the bone mineral density (BMD) of the femurs (Table 2).

TABLE II
PMHS CHARACTERISTICS

Subject	Sex	Age	Cause of Death	Stature (cm)	Mass (kg)	BMI (kg/m^2)	Femur BMD (g/cm^2)
1	F	69	Amyotrophic Lateral Sclerosis	156	49.4	20.5	0.855
2	F	48	Blunt Force Chest Trauma	165	59.0	21.8	1.081
3	F	46	End Stage Renal Disease	156	51.3	21.1	0.798
4	F	70	Acute Respiratory Failure	172	45.4	15.4	0.784
5th Percentile Female [4]				150	50.1	19.6	-
50th Percentile Female [4]				162	72.1	27.7	-

PMHS ages ranged from 46 to 70 years old. Subjects 1 and 3 had near-5th percentile stature and mass. Subject 4 had 5th percentile mass and greater than 50th percentile female stature, and Subject 2 had near-50th percentile stature and near-20th percentile mass. Subject 2 had a normal average femur BMD whereas the other three had BMD values in the osteopenia range [3]. PMHS mass was measured before each testing condition (Table F1). On average, there was an 11.3% reduction in mass after removing the thigh flesh, a 3.2% increase in mass with the addition of the load cell, and a 51.0% decrease in mass after removing the torso. Following testing, a dissection was performed to explicitly define the mass of each component in KTH for use in LPM development (Table F2).

Positioning

For tests where the torso remained intact, subjects were supported using a head strap connected to a drop release mechanism that released upon trigger (Fig. E1). Further, a slacked support rope was used to catch the subject after the event of interest had concluded. Finally, subject positioning was fixed before impact using foam padding between the knees and tape along the lower extremities (Fig. E2). Upon impact, the tape tore, leaving the subject unconstrained. For the ToR condition, a metal rod was inserted into the exposed lumbar spinal segment. This allowed the lumbar spine to be supported by the drop release mechanism to maintain subject positioning for this condition.

The primary focus of positioning was to achieve a neutral, upright seating posture, consistent with the previous study [2]. Using information from the pre-test CT scans, target measurements were obtained to meet this based on pelvis mount positioning and the centre-to-centre knee distance. Knee centre-to-centre distance varied by PMHS in order to keep the thighs (defined for each thigh as the line segment connecting the centre of the femoral head and the midpoint of the medial and lateral femoral epicondyles) parallel. Another focus was maintaining approximately 178 mm between the impacting surface and the subject's knees prior to testing to avoid differences in impact resulting from the input pulse. All recorded positions were within the target ranges (Table 3).

TABLE III
MEASURED POSITIONING PARAMETERS

Measurement	Units	Target	Subject 1	Subject 2	Subject 3	Subject 4
Recline Angle	Deg	90.0 ± 5.0	90.2 ± 1.5	89.9 ± 0.5	89.2 ± 1.2	89.9 ± 0.5
Pelvic Tilt Angle	Deg	0.0 ± 5.0	-0.9 ± 0.7	-2.0 ± 0.4	-1.0 ± 1.5	0.8 ± 0.4
Left Knee Angle	Deg	90.0 ± 5.0	89.8 ± 1.0	89.4 ± 0.7	90.9 ± 1.3	87.9 ± 2.4
Right Knee Angle	Deg	90.0 ± 5.0	92.8 ± 1.1	89.4 ± 0.5	90.3 ± 2.2	87.0 ± 2.9
Knee Center-to-Center	mm	*	165 ± 2	203 ± 1	179 ± 2	168 ± 2
Left Padding-to-Knee	mm	178 ± 5	178 ± 3	177 ± 2	178 ± 3	176 ± 1
Right Padding-to-Knee	mm	178 ± 5	179 ± 2	176 ± 2	178 ± 3	176 ± 2

*Varied by PMHS to keep thighs parallel.

Development of the Lumped Parameter Model

A lumped parameter model (LPM) was created for each PMHS. The modelling method of Rupp and co-authors was adapted to incorporate additional measurements available in the current study (Fig. 2). The model included the masses of the KTH components as well as the elastic, viscous, and frictional interactions between these masses. Individual masses included the mass of the distal femur and knee (mA), the mass of the pelvis (mB), the mass of the pelvis flesh (mC), the mass of the leg below the knee (mD), the mass of the torso (mE), the mass of

the thigh flesh coupled to the distal femur (mF), the mass of the proximal femur (mG), and mass of the thigh flesh coupled to the proximal femur (mH) (Table 4). Masses were obtained via autopsy measurements following the conclusion of the test.

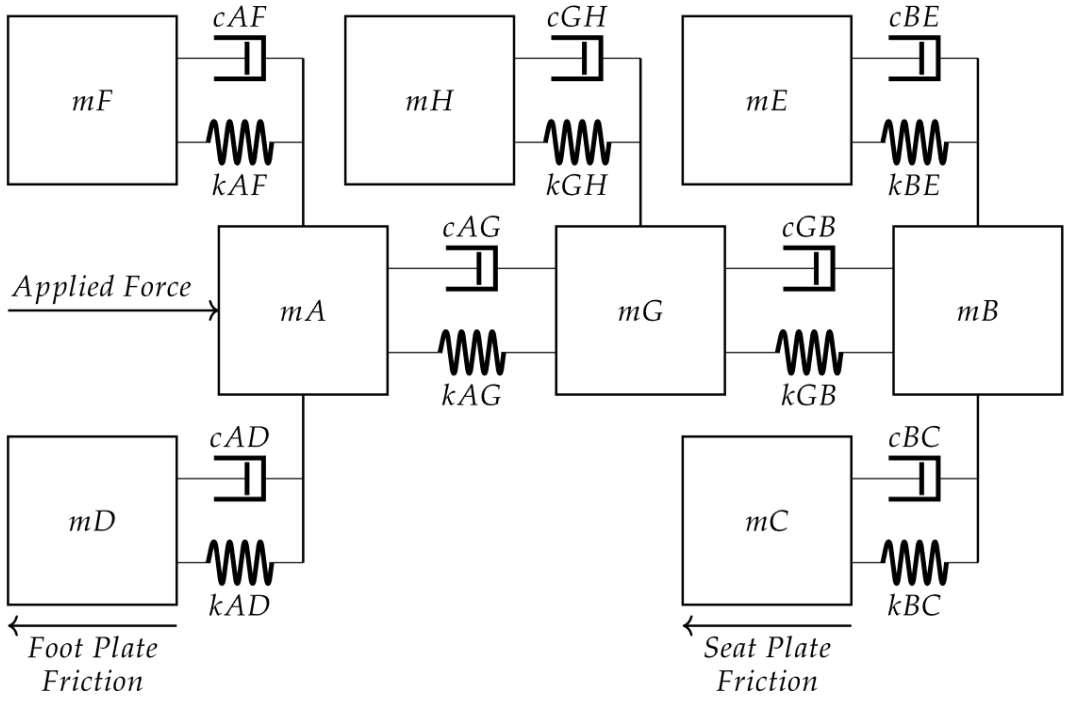

Fig. 2. Lumped parameter model developed to characterize the force transfer along knee-thigh-hip for female PMHSs. Variables correspond to different regions of KTH and include the masses, stiffness, and damping, as well as the frictional interactions between masses.

TABLE IV
LUMPED PARAMETER MODEL MASS DEFINITIONS

Variable	Definition
mA	Average mass of the right and left distal femur, knee, and knee flesh recorded during autopsy
mB	Mass of the pelvis recorded during autopsy
mC	Mass of the pelvis flesh recorded during autopsy
mD	Average mass of the right and left lower legs (below the knee) recorded during autopsy
mE	Mass of the torso recorded during autopsy
mF	Average mass of the right and left thigh flesh recorded during autopsy (half the total measurement to represent distal segment)
mG	Average mass of the right and left proximal femurs recorded during autopsy
mH	Average mass of the right and left thigh flesh recorded during autopsy (half the total measurement to represent proximal segment)

Equation 1 depicts the mathematical representation for a multi-degree-of-freedom system with forcing functions, stiffness, and damping:

$$[M]\{\ddot{x}(t)\} + [c]\{\dot{x}(t)\} + [k]\{x(t)\} = \{F(t)\}, \quad (1)$$

where $[M]$, $[c]$, and $[k]$ are the mass (kg), damping (Ns/m), and stiffness (N/m) matrices, respectively, $\{F(t)\}$ is a vector containing the forces applied to the system (N) obtained during testing as a function of time (applied and frictional forces), and $\{x(t)\}$, $\{\dot{x}(t)\}$, and $\{\ddot{x}(t)\}$ are the position (m), velocity (m/s), and acceleration (m/s^2) vectors of the system as a function of time. Manipulating Equation 1 yields a set of second-order differential equations (Equation 2):

$$\{\ddot{x}(t)\} = [M]^{-1}\{F\} - [M]^{-1}[c]\{\dot{x}(t)\} - [M]^{-1}[k]\{x(t)\}, \quad (2)$$

which can be evaluated at each time step using the applied and frictional forces as inputs. The solution vectors, $\{x(t)\}$ and $\{\dot{x}(t)\}$, containing the displacement and velocity time history of each of the masses in the system, were found using MATLAB® (The MathWorks, Inc.).

Development of the model occurred in the reverse hierarchal order of the experimental tests. By starting with the torso removed tests, where the largest amount of mass was removed from the system, the number of variables tuned for each optimization was minimized. The optimization bounds for each test were developed by starting with the final bounds from the mid-sized male tests [2], then widening the values as necessary such that the tuned variables were generally not approaching the upper or lower limits. Tuned values were obtained for each condition using a pattern search optimization, where the initial conditions of the model were adapted from the final tuned values reported for mid-sized males [2]. After each optimization, multiple surrogate optimizations were run (using the initial conditions, final values, or no initial conditions) to minimize the likelihood of the final solution representing a local minimum. Detailed setup information for the optimization including definitions, assumptions, initial conditions, and the upper and lower bounds can be found in Appendix G.

Upon completion of the LPM for each subject, the force at each mass in the KTH complex was calculated for each knee impact. Femur and hip loading were then characterized by loading rate, maximum force, and loading duration [2]. Overall force transfer, as a percentage of the maximum applied force at the knee, was then calculated for each subject and evaluated for extrinsic variability (posture, impact velocity, impactor type) and intrinsic variability (stature, mass, BMI, mass distribution) for KTH loading.

III. RESULTS

Impact Behaviour

The average knee impact velocities (±SD) for all subjects across all conditions are shown in Fig. 3. All target velocities were within one SD of the average responses. The average impact forces recorded at the knee (±SD) are shown in Fig. 4, where the force is compared as a function of subject condition (Fig. 4A) and impact velocity (Fig. 4B). The average loading characteristics for the impact are reported in Table H1. As the impact velocity was increased, the loading rate and maximum forces consistently showed increasing trends, whereas the time to the maximum force and the loading duration were consistently shortened. Further, across all impact velocities, the WB condition consistently produced the highest loading rate and maximum force while also having the longest time to the maximum force and longest loading duration.

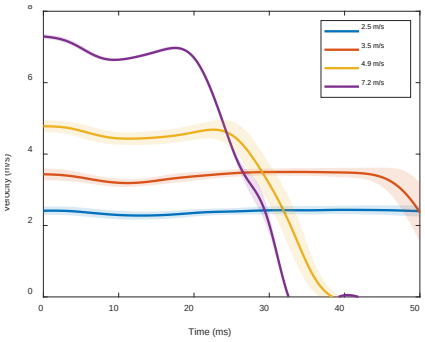

Fig. 3. Average knee impact velocity for all subjects across all conditions ± SD in the response.

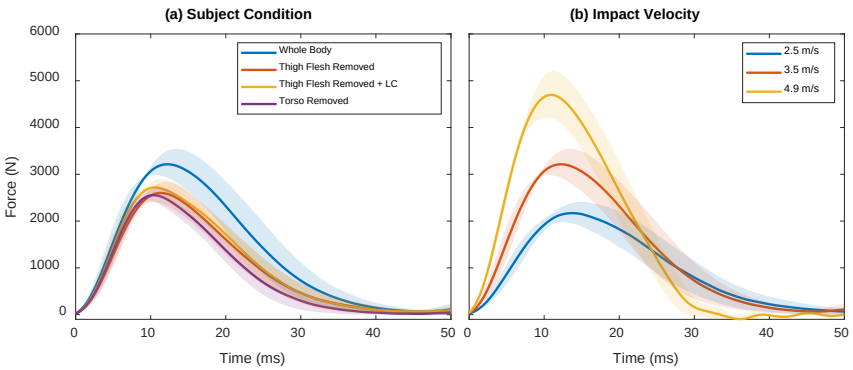

Fig. 4. Average applied knee force for all subjects ± SD in the response. Responses vary by a) subject condition, where only 3.5 m/s impact were used for comparison, and b) impact velocity, where only the WB condition was used for comparison.

Model Predicted Force Transfer

Using the impact behaviour, measured kinematics, and internal loads, subject-specific LPM were developed, and simulations were performed for the ToR condition (Appendix I), TFR+LC condition (Appendix J), TFR condition (Appendix K), and WB condition (Appendix L). Fig. 5. depicts the average LPM inertial responses, defined as the force exerted to accelerate each respective KTH mass component. The force responses of the thigh and pelvis flesh were the largest contributors to inertial losses. Further, the inertial response of the lower leg was found to be similar in magnitude to the torso and femur, while almost double the magnitude of the pelvis. Finally, the torso

consistently exhibited a delayed force response that was relatively small in magnitude compared to the mass percentage it comprised.

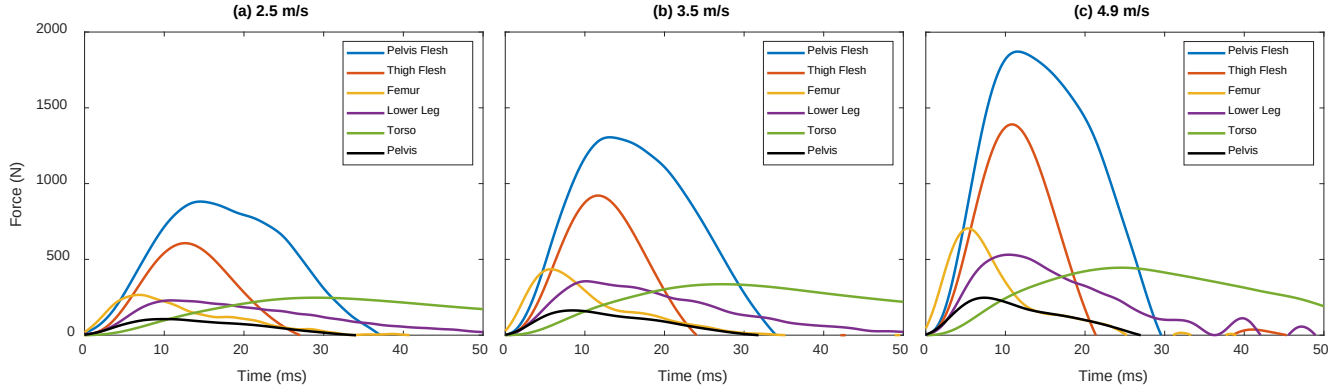

Fig. 5. Average predicted force exerted to accelerate the mass components of KTH by the four subject-specific LPMs, over the duration of the impact for a) 2.5 m/s, b) 3.5 m/s, and c) 4.9 m/s impacts in the WB condition.

Fig. 6 depicts the resulting force transfer after subtracting out the inertial forces, averaged across the four subject-specific LPMs, for each impact velocity in the WB condition. While the increase in impact velocity increased the magnitude of the responses, the force distribution remained consistent. Tables M1-M4 isolate the force transfer along the principal components of KTH for each subject condition and impact velocity. The average force transfer predicted in the WB LPMs was 70.6±1.7% from the knee to the mid-femur and 57.0±3.0% from the knee to the hip. Next, with the removal of the thigh flesh, the average force transfer to the femur and hip increased to 79.2±1.5% and 77.7±1.4%, respectively. The addition of the load cell resulted in a lower percentage of force transferred to the femur and hip with values of 77.0±2.2% and 73.5±2.6%, respectively. Removing the torso showed further decline in the force transfer, as 73.1 ±2.4% of the knee force was transferred to the femur, and 68.8±2.4% was transferred to the hip. Finally, across all subject conditions, the force transfer generally showed a decrease with increasing impact velocity.

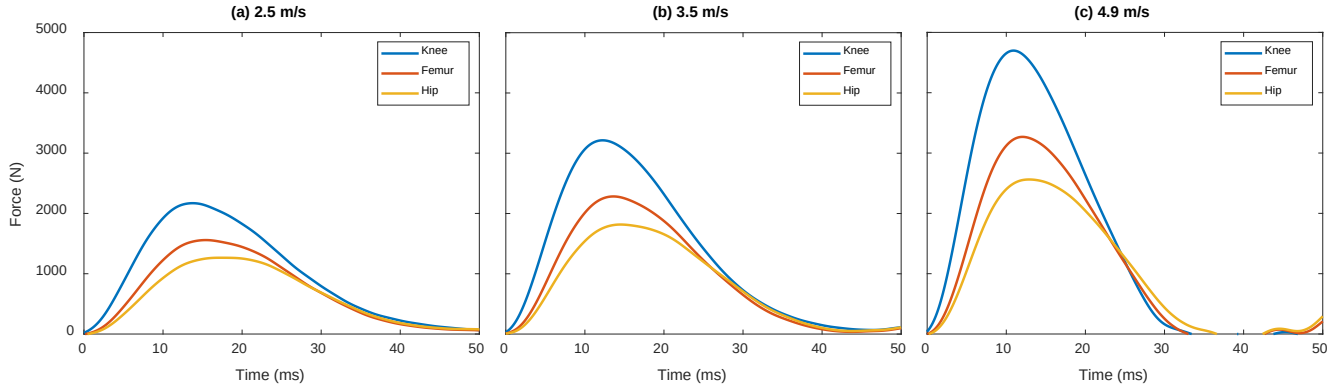

Fig. 6. Average force transfer predicted along KTH by the four subject-specific LPMs, over the duration of the impact for a) 2.5 m/s, b) 3.5 m/s, and c) 4.9 m/s impacts in the WB condition. Note that the knee curve represents the average applied force to the subject, and femur and hip curves represent average LPM predictions.

IV. Discussion

The goal of this study was to quantify the responses of females to KTH impacts. Four female PMHSs were impacted frontally in the knees, and subject-specific lumped parameter models (LPM) were developed from directly measurable responses of the PMHSs in order to quantify responses which were not directly measurable.

Knee Loading Behaviour

The present study aimed to load the KTH complex at a constant velocity; that is, to make the impactor a power source independent of the characteristics of the PMHSs [6]. This also facilitates analysis by minimizing subject-dependent variability on the effect of the input loading. Finally, this is nearest to the intended real-world application of this dataset: the relative velocity between an instrument panel and the occupant in a frontal crash

is likely insensitive to occupant characteristics [7]. To that end, the present study used an impactor with closed-loop feedback to control the velocity throughout the impact event. A constant velocity was best achieved at lower velocities (Fig. 3). Though like previous work combining physical and lumped-parameter methods [2], the LPM development was able to account for variability in the impact velocity time history.

Past studies have concluded that coupling or recruitment of mass to the KTH complex strongly affects the transmission of force and the incidence of injury [2,7]. The knee impact loads of the present study corroborate this: the maximum applied load decreased more after removing the thigh flesh (average 5.4 kg, 11.3% of whole-body mass) than after removing the torso (average 21.6 kg, 51.0% of whole-body mass).

As impact velocity increased, the loading rate, maximum force, and friction force increased, and the time to maximum force and total loading duration decreased (Fig. 4b). This suggests that the KTH complex may be modelled as a dynamic system with inertial, elastic, and dissipative properties. Additionally, the variability of impact load increased with increasing velocity. Assuming consistent extrinsic factors (posture, positioning, impactor velocity), this implies that intrinsic differences (shape, mass distribution) between PMHSs may be frequency dependent.

In order to assess the representation of each impact velocity used in the present study, the Hybrid III midsize male was tested using each impact velocity condition. Table 5 lists the maximum femur force and femur loading rate recorded for each impact velocity. Using the femur loading quantiles reported previously for NCAP and FMVSS 208 tests of 1998-2004 model year vehicles (belted and unbelted), percentiles were calculated for the current knee impact tests [8]. While the loading rates recorded were all within the range of data reported in the regulatory tests, the maximum femur force recorded in the 7.2 m/s test was slightly beyond the 100% percentile (100.7%) indicating that it represents a more extreme impact than what was observed in the regulatory tests for 1998-2004 model year vehicles. Despite this, the 7.2 m/s impact velocity was still used in the analysis as the primary goal was to assess female KTH response across a wider range of impact frequencies. Further, the 7.2 m/s impact velocity was only tested in the final test of the torso removed condition when most of the KTH coupled mass had been removed and the femur force recorded in the female PMHS was a fraction of the Hybrid III midsize male measurement. Finally, due to the age of the vehicle model years tested in the original study, it is currently unknown how each impact velocity compares with the loading information in more recent model year vehicle tests.

TABLE V
HYBRID III MIDSIZE MALE FEMUR LOADING COMPARISON TO REGULATORY TESTS

Impact Velocity (m/s)	Maximum Force (N)	Percentile*	Loading Rate (N/ms)	Percentile*
2.5	3082	32.4%	324	56.5%
3.5	5062	73.3%	652	78.5%
4.9	7563	97.1%	1078	90.4%
7.2	12845	>100%	2075	97.6%

*Values obtained by comparing results to data reported in [8]

Force Transfer Behaviour

In a frontal KTH impact, the force transferred to the hip is less than the applied force [2]. The LPM of the present study predicted the same decrease in force across the skeletal components of the system—the knee, femur, and hip (Fig. 5). The drop in force is related both to the mass being accelerated and to the magnitude of acceleration that mass experiences [9]. The LPMs of the present study show that the masses of the pelvis flesh and thigh flesh were recruited by the acceleration of the skeletal components, and thus participated in the decrease of force from the knee to the hip.

The addition of the thigh flesh into the LPMs represented the greatest source of inertial loss when comparing across test conditions. This behaviour was immediately observable in the impact behaviour where the largest difference in loading characteristics occurred between the WB and TFR test conditions. It was also shown in the resulting force transfer: the addition of the thigh flesh into the model decreased the resulting force transfer from 79.2±1.5% to 70.6±1.7% at the femur and 77.7±1.4% to 57.0±3.0% at the hip. While there was only an average difference of 11.3% in mass when adding the thigh flesh compared to the 51.0% difference with the torso, the thigh flesh was more tightly coupled, and the positioning of it along KTH allowed for a more immediate influence. This concurs with the midsize male LPM [2], for which acetabular force was, on average, 54% of the applied force in the WB condition but roughly 76% in the TFR+LC condition. Therefore, the LPMs suggest that increased thigh flesh decreases the force transferred from the knee to the hip.

In contrast, the LPM suggest that an increased percentage of mass distribution posterior to the hip increases the force transferred from the knee to the hip. Although the current study does not consider occupant bracing and represents a smaller window of subjects compared to real world conditions, subjects with a greater percentage of mass posterior to the hip in the WB condition resulted in a higher percentage of force transferred to the hip (Fig. M1d). Since the pelvis flesh in the LPMs is on the opposite side of the hip from the impacting force, increased mass of pelvis flesh resists acceleration of the hip, and thus permits the increased hip force. This hypothesis takes on additional importance when considering bracing (closer coupling of pelvis flesh [10,11]), habitus (increased overall mass [12]), and sexual dimorphism (mass distribution differences between male and female occupants [13,14]).

The primary adaptation of the LPM methodology from its inception [2] to the present study was in the treatment of the thigh flesh and femur masses. The previous midsize male LPM combined the femur masses distal and proximal to the load cell location, and likewise combined the proximal and distal thigh flesh masses [2]. This permitted a comparison between the effective mass and the measured static mass of the single segments, but it required tuning of the masses at multiple stages in the optimization. In the current study, proximal and distal segments of the femur and thigh flesh were separated. Thus, the masses remained constant throughout testing (with the exception of removing the load cell mass from the femurs) and used values explicitly segmented and defined. This minimized the number of tuned variables by increasing the number of known values. However, any differences between optimization setups were likely accounted for as model development progressed. So, while gross comparisons can be made between the previous and current LPMs, differences in tuned model values between studies should be viewed more as effective response differences and not explicit mechanical property differences.

The torso and lower leg did not strongly affect force transfer (Fig. 5); this agrees with previous findings from a midsize male LPM [2]. The small effect of the torso was also apparent in the physical tests: from TFR+LC to ToR, removing the torso—half the whole-body mass—reduced maximum impact force by only 2-5%. The low contribution of the torso and lower leg was likely due to their geometric decoupling (the centres of mass of those regions were far from the line of action of the impact) and their structural decoupling (low-resistance joints in the absence of muscular activation). The midsize male LPM [2] allowed the coupling of the torso (kBE and cBE) to decrease, but artificially decoupled the lower leg by setting its mass (mD) to a negligible value. The present study used the measured mass of both torso and lower leg. It is possible that spring-and-damper representation of lower leg coupling may enhance LPM accuracy at the periphery of the validation space, i.e., extreme ratios of lower leg to KTH mass.

Studies of KTH injury have found that injury location depends on the duration and rate of loading: high-rate short-duration loads (often from rigid impactors) caused injury to the knee and distal femur [15,16], while low-rate long-duration loads (often from padded impactors) caused injury to the hip and proximal femur [7]. This rate dependence suggests that the effective coupling between the knee and hip should be expected to change when moving from a slow-loading regime well below the natural frequency, where the KTH system behaves more coupled, to a fast-loading regime at or above the natural frequency, where the KTH behaves more decoupled. To explore this possibility, the current study included a higher velocity impact (7.2 m/s) than the previous study on midsize males [2]. This assumed that the natural frequency of the KTH system scaled with the effective dynamic mass: i.e., since the mass of the small female is less than that of the midsize male, the natural frequency of the small female KTH would be higher than that of the midsize male. While this may be true when considering uniformly scaled occupants, sex-based differences in mass distribution may add nuance to this simple model. For example, comparing the females of the present study with the midsize males of the previous study [2], the ratios of thigh flesh mass (0.5) and pelvis (with pelvis flesh) (0.8) suggest that uniform scaling of occupant geometry may not be valid.

Development of the LPMs

Model development occurred in reverse order of testing beginning with the ToR tests (Appendix I), then introducing the torso into the model with the TFR+LC Tests (Appendix J), followed by accounting for the effect of the load cell (Appendix K), and finally, introducing the thigh flesh into the model (Appendix L). Generally, the models were able to accurately capture the subject kinematics measured experimentally, though they were most accurate within the first 20-25 ms of impact. This is a result of the objective function for optimization which favoured the immediate loading and unloading phases of the impact. While increasing the bounds of the optimization to encompass more of the impact would theoretically increase the overall accuracy of the system, it would also remove parameter weighting from the initial impact and ultimately detract from the main parameter

of interest in the model – the force transfer along KTH, which is represented by the maximum values along KTH. Thus, while larger differences arose between the model and the experimental testing at later time periods, the current method of optimization provides the authors with higher levels of confidence that the maximum force and acceleration values are most accurately represented in the final WB LPMs.

The overall steps in the optimization also showed slight variations. Current LPM development began with the ToR tests, whereas the previous study started with TFR+LC tests. The justification for the current process was that the optimization started in the simplest test condition with the largest amount of KTH mass removed, and mass segments were introduced to limit the number of tuned parameters for each optimization. It is suspected that justification for beginning the optimization with TFR+LC tests arises from the findings that there was increased pelvis rotation in the ToR test condition. Once again, since the behaviour was likely accounted for in subsequent optimizations, differences in the tuned values of the LPMs between test studies should be treated as effective response differences and not explicit mechanical property differences.

Throughout all subject conditions, there was a large magnitude of oscillatory pelvis pitch displacement (pelvis rocking) observed in the experimental tests. This led to a large increase in the variability of the pelvis accelerations. This behaviour was accentuated at higher impact velocities. For the one-dimensional LPM, rotation was not an available input, and thus was estimated in the model through a decrease in coupling of adjacent masses. With the final tuned values, increased rotation generally correlated with lower maximum pelvis accelerations. Further, this also affected the resulting force transfer, as increased pelvis rotation during the tests generally correlated with a decrease in the force transferred to the hip. Although observable in each subject condition, the behaviour was most pronounced in the ToR tests, where the magnitudes were larger, and the rotation occurred earlier. Removing the mass of the torso allowed for greater pelvis rotation and the largest decrease between test conditions when removing mass from KTH. This would seemingly indicate that the torso plays a large role in stabilizing the pelvis in the KTH response, though the findings would suggest that this poses greater injury risk as it increases the force transfer to the hip.

Inclusion of load cells under the seat plate and foot plate of the test rig allowed subject interaction with the plates to be measured and incorporated into the model. For LPM development, friction was defined by inertially compensating the shear forces as the subject moved along each plate. While a reasonable definition for a majority of the testing duration, possible errors did arise in the seat friction values whenever the subject's lower leg contacted the edge of the seat plate during testing. This behaviour was mainly present in higher velocity tests and occurred long after the maximum values; however, it is possible that this was a factor in some of the force deviations in the model present at later time points. Additionally, while the effective contribution of the lower leg was assumed to be minimal in previous work [2], current model findings suggest that the lower leg does absorb some of the force from the impact, with a predicted force contribution in KTH similar to that of the torso. The mechanism for force absorption appears to result from heel contact that increases as more knee extension occurs during the impact and the femur dips in the z-direction.

The PMHS tests used to develop the midsize male LPM used different impactor padding at their lowest velocity (1.2 m/s) [2]. Though the 1.2 m/s test velocity was used in the mid-sized male tests, the 3.5 m/s and 4.9 m/s impacts remained consistent between test setups. In the present study, the padding used in all four velocities (2.5, 3.5, 4.9, and 7.2 m/s) remained unchanged. Future work should consider this when using the results of these studies.

Future Work

The present study is the first to have performed whole body KTH impacts on female PMHSs. The findings of this study suggest that sex-based intrinsic factors affect the dynamic response of the KTH system. However, more work is needed to identify and quantify the sensitivity of KTH load transfer to intrinsic occupant factors, especially those strongly correlated with sex: mass distribution [13,14], bone shape [17-20], skeletal alignment [21], joint stiffness and range of motion [22-24], and more. Experiments with PMHSs, enhanced by LPMs, help to answer many of the outstanding questions. However, future work should aim to utilize the PMHSs and LPMs to develop and validate female KTH finite element models (FEM). Upon validation of the FEM in test conditions similar to those conducted in the present study, the FEM may then be further altered to better examine the effects of intrinsic variability (stature, mass, BMI, mass distribution) in frontal impacts. Additionally, future work should also utilize the newly developed LPMs to evaluate the feasibility of current KTH injury risk functions for females with the possibility for updated recommendations.

Future work should also examine the sensitivity of the small female KTH system to extrinsic variability. Past PMHS studies have explored variations in posture [25-27]. The one-dimensional nature of the LPM in the present

study precludes explicit consideration of posture, and combined PMHS, LPM, and FEM analysis would help to assess the uncertainties and small variations in PMHS positioning. For example, although a consistent positioning procedure was implemented, past studies have shown a sensitivity of load transfer to pelvis orientation [2,10,11]. Similarly, the removal of the torso in the present study was found to reduce constraint on pelvis rotation during the impact, although the torso mass did not strongly affect KTH force transfer.

Lastly, future work should examine the effects of muscle bracing on small female KTH load transfer. Muscle bracing has been predicted to affect overall occupant restraint [28], femur force [29], and KTH force transfer [10,11]. However, it is unknown whether these predictions are affected by sex-related differences.

V. CONCLUSIONS

This study analysed the loading and kinematic responses of four female PMHSs tested in a bilateral knee-impact test condition in order to develop subject-specific LPMs. The average force transfer predicted in the WB LPMs was 70.6±1.7% from the knee to the mid-femur and 57.0±3.0% from the knee to the hip. PMHS and LPM findings highlighted the importance of the relative masses of the skeletal and non-skeletal components of the KTH system. Development of the LPMs is an important and necessary first step in characterizing the female KTH response. The results of this study provide a path for future validation of female KTH finite element models to further examine the effects of extrinsic and intrinsic variability in frontal impacts.

VI. ACKNOWLEDGEMENT

The following research was funded by the National Highway Traffic Safety Administration (NHTSA) under contract number DTNH2215D00022. The authors would also like to thank the staff at the University of Virginia's Center for Applied Biomechanics, USA, for all their help in this test series.

VII. REFERENCES

[1] Sochor M and Rupp J. Commentary: Emergency Department Patients and Crash Test Dummies: What Do They Have in Common? *Annals of Emergency Medicine*, 2005. 46(2): p. 169-171

[2] Rupp JD, Miller CS, et al. Characterization of knee-thigh-hip response in frontal impacts using biomechanical testing and computational simulations. *Stapp Car Crash J*, 2008. 52: p. 421-74

[3] Kanis JA. Assessment of fracture risk and its application to screening for postmenopausal osteoporosis: synopsis of a WHO report. WHO Study Group. *Osteoporos Int*, 1994. 4(6): p. 368-81

[4] Fryar CD, Gu Q, Ogden CL, and Flegal KM. Anthropometric Reference Data for Children and Adults: United States. 2016, National Center for Health Statistics: Vital and Health Statistics.

[5] Rudd R, Kerrigan J, Crandall J, and Arregui C. Kinematic Analysis of Head/Neck Motion in Pedestrian-Vehicle Collisions Using 6-Degree-of-Freedom Instrumentation Cubes. 2006, SAE International.

[6] Subit D, Duprey S, et al. Response of the human torso to lateral and oblique constant-velocity impacts. *Annals of advances in automotive medicine. Association for the Advancement of Automotive Medicine*, 2010. 54: p. 27-40

[7] Melvin J and Nusholtz G. Tolerance and response of the knee-femur-pelvis complex to axial impacts—impact sled tests. 1980, The University of Michigan: Highway Safety Research Institute.

[8] Rupp JD, Miller CS, et al. Characterization of Knee Impacts in Frontal Crashes. *Proceedings* 2007.

[9] Newton I, "Philosophiae naturalis principia mathematica". 1687: Londini: Jussu Societatis Regiæ.

[10] Chang CY, Rupp JD, Reed MP, Hughes RE, and Schneider LW. Predicting the effects of muscle activation on knee, thigh, and hip injuries in frontal crashes using a finite-element model with muscle forces from subject testing and musculoskeletal modeling. *Stapp Car Crash J*, 2009. 53: p. 291-328

[11] Chang CY, Rupp JD, Kikuchi N, and Schneider LW. Development of a finite element model to study the effects of muscle forces on knee-thigh-hip injuries in frontal crashes. *Stapp Car Crash J*, 2008. 52: p. 475-504

[12] Reed MP, Ebert-Hamilton SM, and Rupp JD. Effects of obesity on seat belt fit. *Traffic Inj Prev*, 2012. 13(4): p. 364-72

[13] Taylor RW, Grant AM, Williams SM, and Goulding A. Sex differences in regional body fat distribution from pre- to postpuberty. *Obesity (Silver Spring)*, 2010. 18(7): p. 1410-6

[14] Bredella MA. Sex Differences in Body Composition. *Adv Exp Med Biol*, 2017. 1043: p. 9-27

[15] Powell WR, Ojala SJ, Advani SH, and Martin RB. Cadaver Femur Responses to Longitudinal Impacts. 1975, SAE International.

[16] Melvin J and Stalnaker R. Tolerance and response of the knee-femur-pelvis complex to axial impact. 1976, The University of Michigan: Highway Safety Research Institute.
[17] Wang SC, Brede C, et al. Gender differences in hip anatomy: possible implications for injury tolerance in frontal collisions. *Annual proceedings. Association for the Advancement of Automotive Medicine*, 2004. 48: p. 287-301
[18] Seeman E. Bone quality: the material and structural basis of bone strength. *J Bone Miner Metab*, 2008. 26(1): p. 1-8
[19] Riggs BL, Melton III LJ, 3rd, et al. Population-based study of age and sex differences in bone volumetric density, size, geometry, and structure at different skeletal sites. *J Bone Miner Res*, 2004. 19(12): p. 1945-54
[20] Holcombe S and Wang S. Subcutaneous Fat Distribution in the Human Torso, in *Proceedings of the International Research Council on the Biomechanics of Impact (IRCOBI)*. 2014: Berlin, Germany. p. 389-396.
[21] Nguyen AD and Shultz SJ. Sex differences in clinical measures of lower extremity alignment. *J Orthop Sports Phys Ther*, 2007. 37(7): p. 389-98
[22] Shultz SJ, Sander TC, Kirk SE, and Perrin DH. Sex differences in knee joint laxity change across the female menstrual cycle. *The Journal of sports medicine and physical fitness*, 2005. 45: p. 594
[23] Hobara H, Kato E, Kobayashi Y, and Ogata T. Sex differences in relationship between passive ankle stiffness and leg stiffness during hopping. *J Biomech*, 2012. 45(16): p. 2750-4
[24] Hwang J and Jung MC. Age and sex differences in ranges of motion and motion patterns. *Int J Occup Saf Ergon*, 2015. 21(2): p. 173-86
[25] Rupp J, Reed M, Jeffreys T, and Schneider L. Effects of hip posture on the frontal impact tolerance of the human hip joint. 2003. p. 21-33.
[26] Salzar RS, Bass CR, et al. Development of Injury Criteria for Pelvic Fracture in Frontal Crashes. *Traffic Injury Prevention*, 2006. 7: p. 299-305
[27] Meyer EG and Haut RC. The effect of impact angle on knee tolerance to rigid impacts. *Stapp Car Crash J*, 2003. 47: p. 1-19
[28] Armstrong RW. Human Muscular Restraint During Sled Deceleration, H.P. Waters, Editor. 1968, SAE International. p. 3163-3174.
[29] Bose D and Crandall JR. Influence of active muscle contribution on the injury response of restrained car occupants. 2008. p. 61-72.

VIII. APPENDIX

Appendix A: Test Images

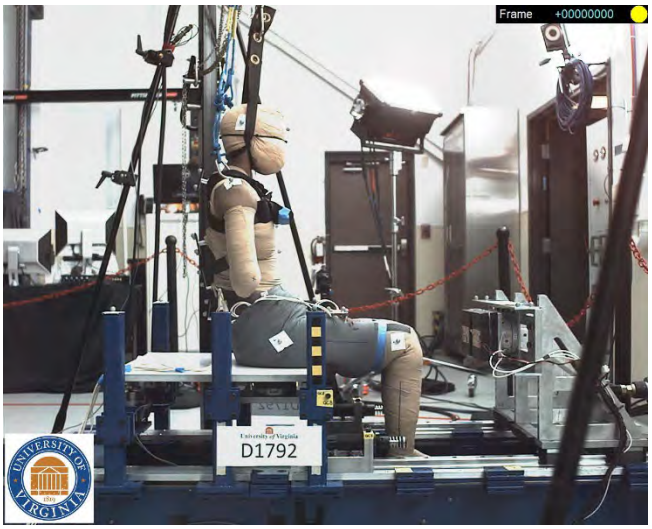

Fig. A1. Example setup of the whole body (WB) test condition obtained from high-speed video.

Fig. A2. Example setup of the thigh flesh removed (TFR) test condition obtained from high-speed video.

Fig. A3. Example setup of the thigh flesh removed plus load cell (TFR+LC) test condition obtained from high-speed video.

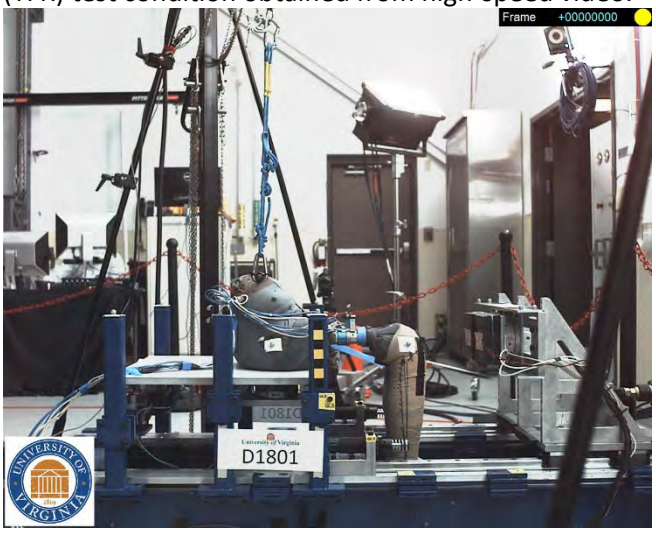

Fig. A4. Example setup of the torso removed (ToR) test condition obtained from high-speed video.

Appendix B: Subject Preparation for WB Tests

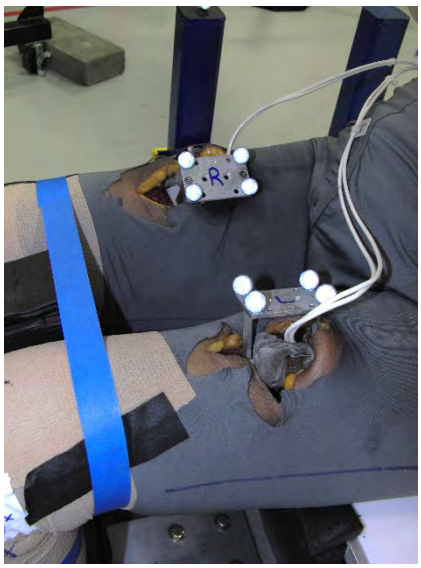

Fig. B1. Lateral "T" cuts made in the specimen to insert femur hose clamp mounts, accelerometers, and motion tracking plates.

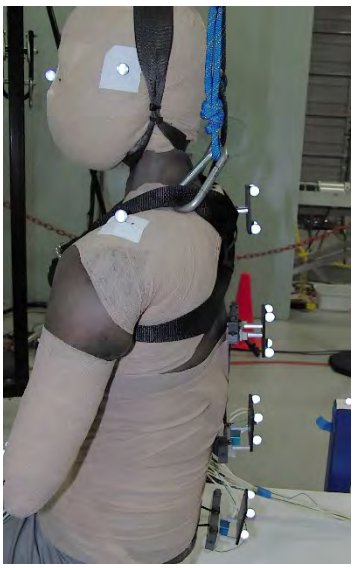

Fig. B2. T1, T8, L2, and pelvis mount positioning on test day used to track the subject's orientation.

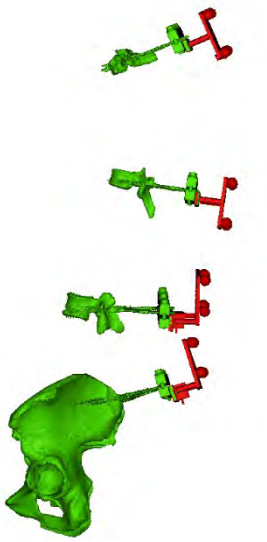

Fig. B3. 3D reconstruction of the T1, T8, and L2 vertebral bodies and the pelvis, obtained from CT imaging. This was used to track mount integrity and positioning during testing.

Appendix C: Subject Preparation for TFR Tests

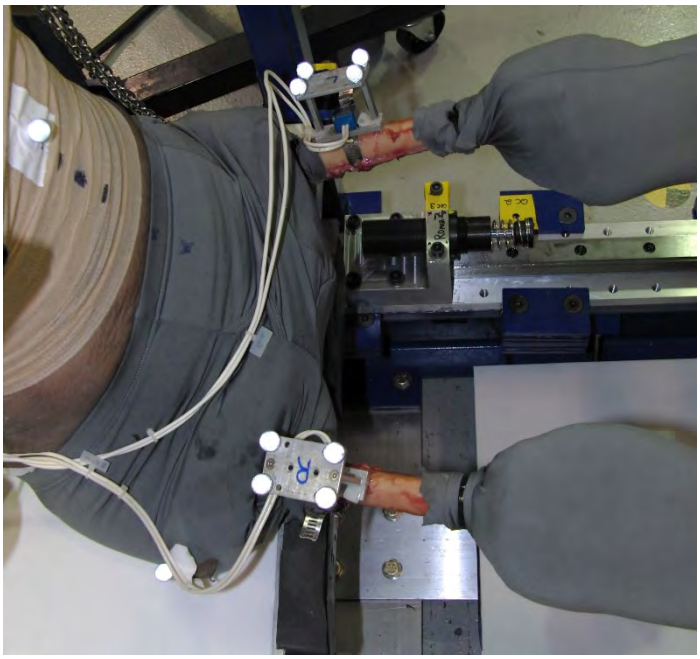

Fig. C1. Appearance of the subject following the removal of the thigh flesh.

Appendix D: Subject Preparation for TFR+LC Tests

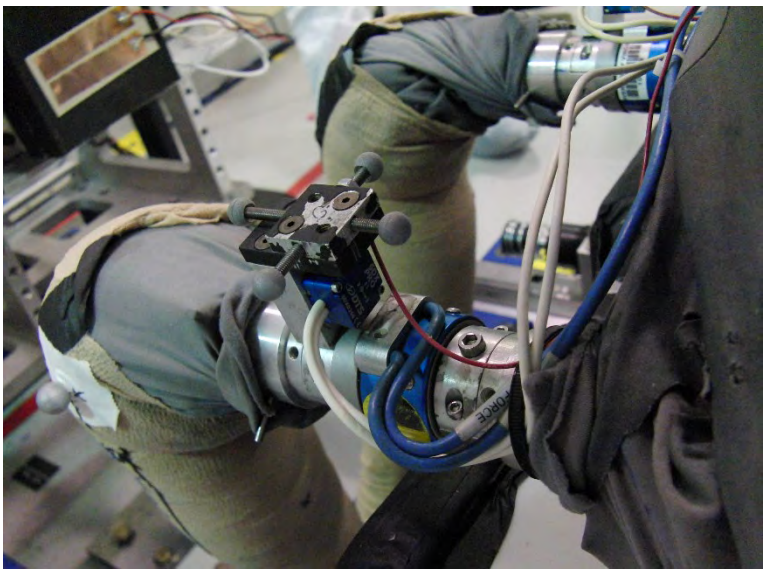

Fig. D1. Close-up view of the left femur following the addition of the femur load cells.

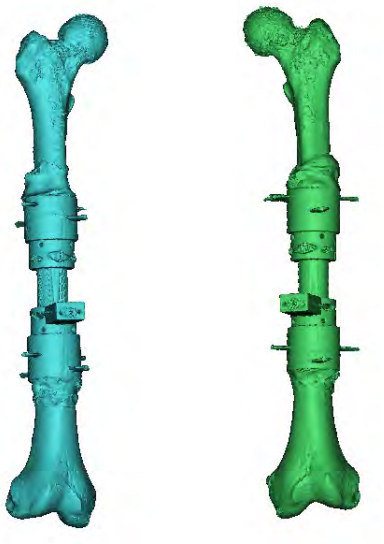

Fig. D2. 3D reconstruction obtained from CT imaging of the femurs with the femur load cells.

Appendix E: Subject Support

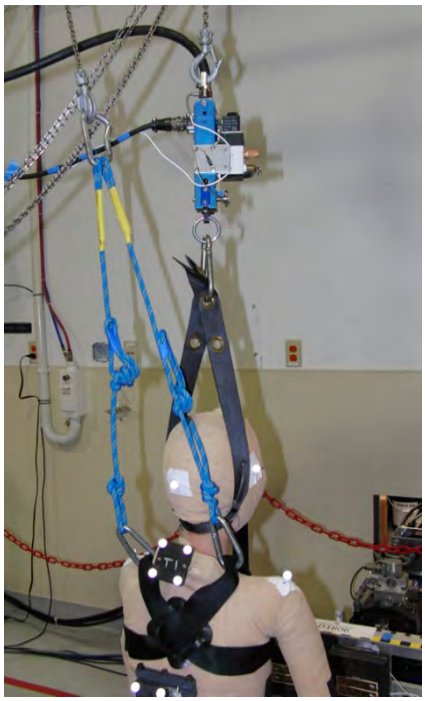

Fig. E1. Support system used for maintaining subject positioning prior to each test and catching the subject after the event of interest had concluded.

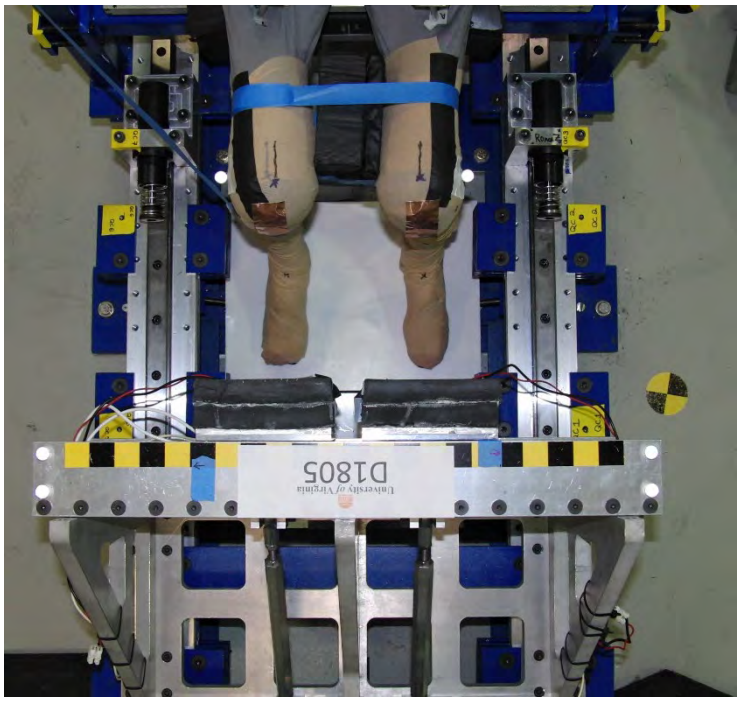

Fig. E2. Foam and tape orientation used to maintain subject positioning prior to impact. Prior to each test, slits were cut into the tape so that it tore immediately upon impact.

Appendix F: Body Segment Masses

TABLE F.I
SUBJECT MASS FOR EACH TEST CONDITION

Subject	Whole body (kg)	Thigh Flesh Removed (kg)	Thigh Flesh Removed Plus Load Cell (kg)	Torso Removed (kg)
1	43.00	38.52	39.84	18.52
2	54.59	47.61	48.91	23.05
3	49.46	43.52	44.81	23.04
4	37.40	34.02	35.32	18.09
Average (±SD)	46.11 (±7.50)	40.92 (±5.91)	42.22 (±5.91)	20.67 (±2.74)

TABLE F.II
BODY SEGMENT MASSES

Subject	Torso (kg)	Pelvis (kg)	Pelvis Flesh (kg)	Thigh Flesh (kg)		Femur (kg)		Knee (kg)		Below knee (kg)	
				Left	Right	Left	Right	Left	Right	Left	Right
1	21.32	1.48	9.05	2.17	2.31	0.60	0.54	1.10	1.18	1.94	1.82
2	25.85	1.25	13.45	3.58	3.40	0.60	0.61	1.00	0.94	2.21	2.23
3	21.77	1.15	11.83	2.85	3.09	0.57	0.61	1.12	1.37	2.92	2.74
4	17.24	1.30	9.63	1.61	1.77	0.62	0.63	0.86	0.83	1.70	1.79
Average (±SD)	21.55 (±3.52)	1.30 (±0.12)	10.99 (±1.76)	2.60 (±0.69)		0.60 (±0.03)		1.05 (±0.17)		2.17 (±0.42)	

Appendix G: LPM Definitions and Initial Conditions

Table G1 lists all tuned variables through the stages of the optimization, along with definitions, initial conditions, and upper and lower bounds. For tests in the ToR condition, the masses mA, mB, mC, mD, and mG were known, while the eight stiffness and damping values connecting these masses (kAG, cAG, kGB, cGB, kBC, cBC, kAD, and cAD) were unknown and determined via optimization. Masses mE, mF, and mH were effectively removed from the model since the torso, distal thigh flesh, and proximal thigh flesh, respectively, were not present in the ToR condition.

The optimization window for all tests included the time when the applied force first reached 15% of the maximum recorded value to the time when the value last fell below 50% of the maximum value [2]. Tuned values for the ToR condition, where the femur load cells were present, were determined using the following function (Equation G1):

$$Optimization\ function = \min\{\sum_{i=1}^{2}[2 * (NRMSE_{Femur\ \ Force_i}) + 2 * (NRMSE_{Hip\ Force_i}) + 0.5 * (NRMSE_{Distal\ \ Femur\ \ Acc_i}) + 0.5 * (NRMSE_{Proximal\ \ Femur\ \ Acc_i}) + 0.5 * (NRMSE_{Pelvis\ Force_i})]\}, \quad \text{(G1)}$$

where the root mean square error (RMSE) between the experimental data and model predicted values were obtained and then normalized by the respective maximum recorded experimental values to obtain the normal root mean square error (NRMSE). The NRMSE values were summed for the 3.5 m/s ($i = 1$) and 4.9 m/s ($i = 2$) impacts in each condition. Data used include the accelerations at the pelvis and distal and proximal femur, the femur force obtained via the femur load cell, and the hip force. Note that the hip force was calculated by performing an inertial compensation of the femur load cell using the proximal femur acceleration and the mass between the centre of the load cell and the hip, as reported previously [2]. Since the primary goal of the model was to output the force transfer along KTH, force measurements were assigned larger parameter weighting than accelerations.

Following the completion of the ToR model, the final values, including measured and tuned, were held constant and inputted into the TFR+LC model. With the addition of the torso into the model, the mass of mE was now known, leaving only the spring and damper interactions between the torso and the pelvis as unknowns that were determined via optimization. Note that masses mF and mH were still removed from the model as the thigh flesh

remained absent in the TFR+LC condition. Since the femur load cells were still present in the TFR+LC condition, values were also tuned using the optimization function provided in Equation 3.

While no variables were tuned in the TFR condition, it marked the transition period where the femur load cells were no longer present in the experimental testing. To account for this change in the model, the masses of the distal and proximal femurs (denoted mA and mG, respectively) were updated by removing half the mass of the femur load cell from each mass and replacing it with half the mass of the femur segment that was removed. Hence, the TFR model operates under the assumption that the effect of load cell removal can be sufficiently described by altering the masses and not the stiffness and damping values, an assumption consistent with the previously developed LPM for mid-sized males [2]. With the updated values, the TFR model was run to examine the behaviour of the model in relation to the TFR+LC condition.

After updating the model to account for the removal of the load cell, the values were inputted into the WB model as known values. With the addition of the thigh flesh into the model, the masses of mF and mH were now known, leaving only the stiffness and damping interaction between the thigh flesh and femur as unknowns that were determined via optimization. Thus, it was assumed that the mass of the thigh flesh was distributed equally between the proximal and distal segments (mF and mH), and the stiffness and damping of the two segments were equivalent (kAF and cAF assumed equivalent to kGH and cGH).

Since femur load cells were no longer present, Equation G2 was updated to obtain the tuned values for the WB condition (Equation G2):

$$Optimization\ function = \min\{\sum_{i=1}^{2}[0.5 * (NRMSE_{Distal\ \ Femur\ \ Acc_i}) + 0.5 * (NRMSE_{Proximal\ \ Femur\ \ Acc_i}) + 0.5 * (NRMSE_{Pelvis\ \ Force_i})]\}, \quad \text{(G2)}$$

where only the acceleration data was used in the optimization function, and all other equation definitions remained consistent.

TABLE G.I
LUMPED PARAMETER MODEL OPTIMIZATION

Model Parameter	Definition	Initial Conditions	Lower Bound of Optimization	Upper Bound of Optimization
kAG	Stiffness and damping of femur	425,000 N/m	200,000 N/m	600,000 N/m
cAG		1500 Ns/m	500 Ns/m	10,000 Ns/m
kGB	Stiffness and damping of proximal femur and pelvis	55,000 N/m	20,000 N/m	700,000 N/m
cGB		10690 Ns/m	500 Ns/m	11,000 Ns/m
kBC	Stiffness and damping of connection between pelvis and pelvis flesh	37610 N/m	3000 N/m	200,000 N/m
cBC		600 Ns/m	250 Ns/m	5,000 Ns/m
kAD	Stiffness and damping of distal femur/knee and lower leg	15 N/m	10 N/m	3,000 N/m
cAD		300 Ns/m	50 Ns/m	1,000 Ns/m
kBE	Stiffness and damping of the connection between pelvis and torso	15 N/m	1 N/m	500 N/m
cBE		35 Ns/m	1 Ns/m	500 Ns/m
kAF	Stiffness and damping of the connection between the distal femur and thigh flesh	128,190 N/m	1,000 N/m	500,000 N/m
cAF		500 Ns/m	50 Ns/m	10,000 Ns/m
kGH	Stiffness and damping of the connection between the proximal femur and thigh flesh	128,190 N/m	1,000 N/m	500,000 N/m
cGH		500 Ns/m	50 Ns/m	10,000 Ns/m

Appendix H: Knee Loading Characteristics

TABLE H.I
KNEE LOADING CHARACTERISTICS FOR 2.5 M/S IMPACTS

Subject Condition	Subject	Loading Rate (N/ms)	Loading Duration (ms)	Time to Peak Force (ms)	Maximum force (kN)
WB	1	258	33.2	12.2	2.10
	2	253	33.4	14.3	2.44
	3	220	39.6	15.5	2.29
	4	256	29.7	11.8	1.98
	Average (±SD)	247 (±18)	34.0 (±4.1)	13.5 (±1.8)	2.20 (±0.20)
TFR+LC	1	238	31.4	12.0	1.87
	2	260	30.5	11.6	1.98
	3	204	38.5	14.2	1.88
	4	241	29.2	10.7	1.67
	Average (±SD)	236 (±23)	32.4 (±4.2)	12.1 (±1.5)	1.85 (±0.13)

TABLE H.II
KNEE LOADING CHARACTERISTICS FOR 3.5 M/S IMPACTS

Subject Condition	Subject	Loading Rate (N/ms)	Loading Duration (ms)	Time to Peak Force (ms)	Maximum force (kN)
WB	1	432	29.5	10.9	3.09
	2	388	30.5	13.8	3.47
	3	407	33.1	12.8	3.52
	4	430	25.7	10.5	2.96
	Average (±SD)	414 (±21)	29.7 (±3.1)	12.0 (±1.6)	3.26 (±0.28)
TFR	1	325	27.8	11.8	2.64
	2	365	28.6	11.2	2.72
	3	362	32.0	12.1	2.78
	4	372	25.8	9.6	2.36
	Average (±SD)	356 (±21)	28.6 (±2.6)	11.2 (±1.1)	2.63 (±0.19)
TFR+LC	1	419	28.8	10.2	2.77
	2	403	28.0	10.7	2.80
	3	377	32.2	11.7	2.88
	4	417	25.5	9.1	2.57
	Average (±SD)	404 (±20)	28.6 (±2.8)	10.4 (±1.1)	2.75 (±0.13)
ToR	1	373	24.3	9.9	2.48
	2	393	27.4	10.4	2.69
	3	369	28.8	11.4	2.69
	4	396	24.0	9.4	2.44
	Average (±SD)	383 (±14)	26.1 (±2.4)	10.3 (±0.9)	2.57 (±0.14)

TABLE H.III
KNEE LOADING CHARACTERISTICS FOR 4.9 M/S IMPACTS

Subject Condition	Subject	Loading Rate (N/ms)	Loading Duration (ms)	Time to Peak Force (ms)	Maximum force (kN)
WB	1	647	25.1	10.6	4.44
	2	677	24.2	11.2	5.15
	3	668	26.5	11.2	5.10
	4	644	23.4	10.2	4.14
	Average (±SD)	659 (±16)	24.8 (±1.3)	10.8 (±0.5)	4.71 (±0.5)
TFR+LC	1	666	24.6	8.9	3.96
	2	579	23.8	9.8	3.77
	3	647	25.7	10.0	4.24
	4	673	23.3	8.1	3.71
	Average (±SD)	642 (±43)	24.4 (±1.0)	9.2 (±0.9)	3.92 (±0.24)
ToR	1	659	21.5	8.5	3.83
	2	680	24.3	8.6	3.95
	3	612	25.1	9.5	3.88
	4	658	21.8	8.1	3.63
	Average (±SD)	652 (±28)	23.2 (±1.8)	8.7 (±0.6)	3.82 (±0.14)

TABLE H.IV
KNEE LOADING CHARACTERISTICS FOR 7.2 M/S IMPACTS

Subject Condition	Subject	Loading Rate (N/ms)	Loading Duration (ms)	Time to Peak Force (ms)	Maximum force (kN)
ToR	1	1145	19.0	7.7	6.06
	2	1201	20.8	7.6	6.28
	3	1230	21.0	7.3	6.11
	4	1167	20.0	7.1	5.72
	Average (±SD)	1186 (±37)	20.2 (±0.9)	7.4 (±0.3)	6.04 (±0.24)

Appendix I: Torso Removed Condition

TABLE I.I
TORSO REMOVED MODEL

Model Parameter	Subject 1	Subject 2	Subject 3	Subject 4
mA	1.510 kg	1.333 kg	1.611 kg	1.213 kg
mB	0.742 kg	0.626 kg	0.576 kg	0.650 kg
mC	4.527 kg	6.725 kg	5.916 kg	4.815 kg
mD	1.879 kg	2.218 kg	2.830 kg	1.746 kg
mE	--	--	--	--
mF	--	--	--	--
mG	0.603 kg	0.624 kg	0.585 kg	0.621 kg
mH	--	--	--	--
kAG	457768 N/m	572456 N/m	441384 N/m	490536 N/m
cAG	2364 Ns/m	4316 Ns/m	5340 Ns/m	1468 Ns/m
kGB	444120 N/m	38616 N/m	661208 N/m	259800 N/m
cGB	1904 Ns/m	3120 Ns/m	976 Ns/m	1040 Ns/m
kBC	141034 N/m	187114 N/m	88810 N/m	3050 N/m
cBC	1184 Ns/m	1080 Ns/m	1064 Ns/m	2616 Ns/m
kAD	15 N/m	15 N/m	15 N/m	11 N/m
cAD	195 Ns/m	220 Ns/m	204 Ns/m	236 Ns/m
kBE	--	--	--	--
cBE	--	--	--	--
kAF	--	--	--	--
cAF	--	--	--	--
kGH	--	--	--	--
cGH	--	--	--	--

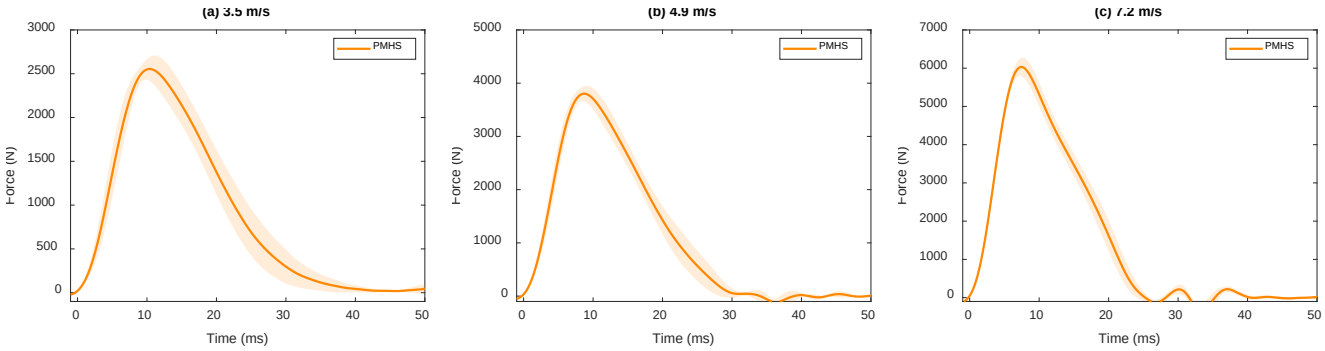

Fig. I1. Average Knee force recorded by the left and right impactor load cells for all subjects ± SD for a) 3.5 m/s, b) 4.9 m/s, and c) 7.2 m/s impacts.

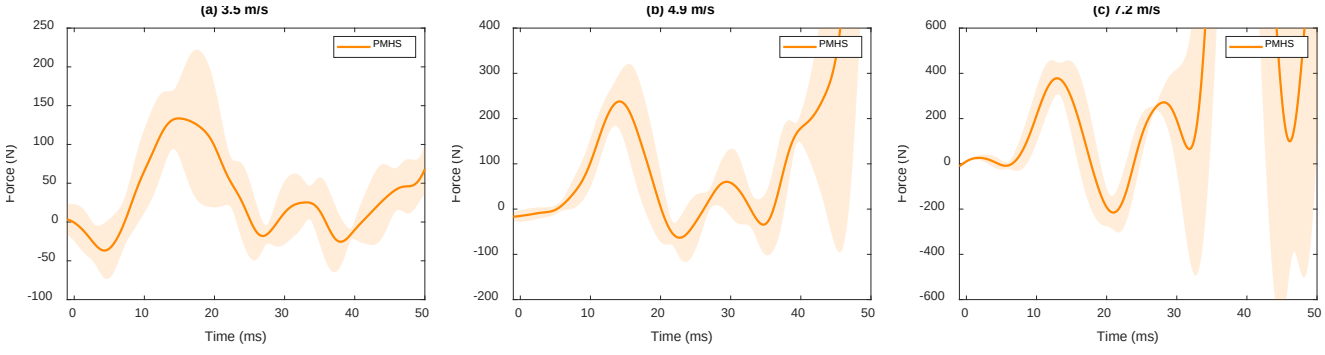

Fig. I2. Average seat friction force for all subjects ± SD for a) 3.5 m/s, b) 4.9 m/s, and c) 7.2 m/s impacts.

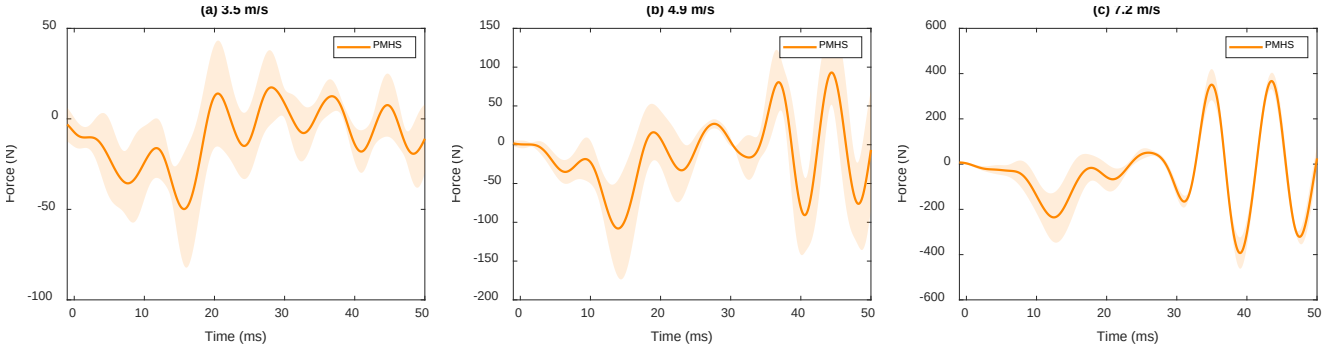

Fig. I3. Average foot friction force for all subjects ± SD for a) 3.5 m/s, b) 4.9 m/s, and c) 7.2 m/s impacts.

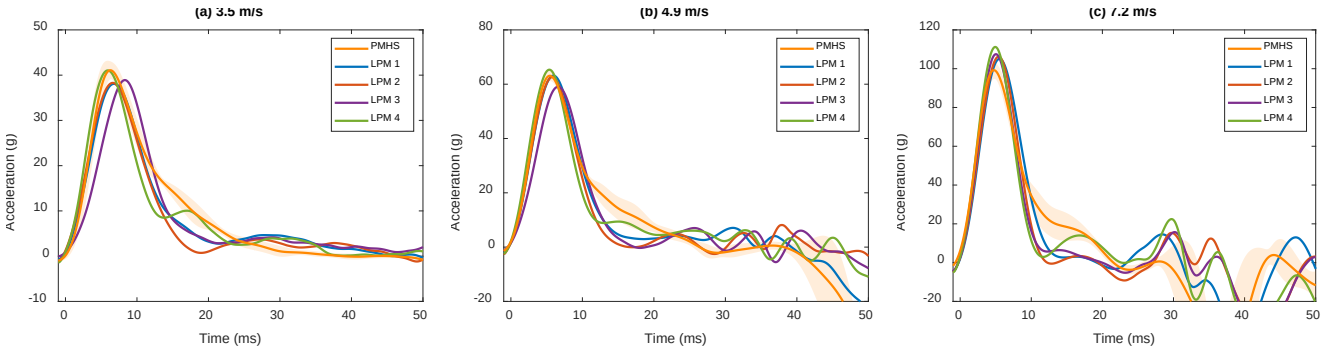

Fig. I4. Average femur acceleration for all subjects ± SD compared with the individual subject responses predicted by the lumped parameter model for a) 3.5 m/s, b) 4.9 m/s, and c) 7.2 m/s impacts.

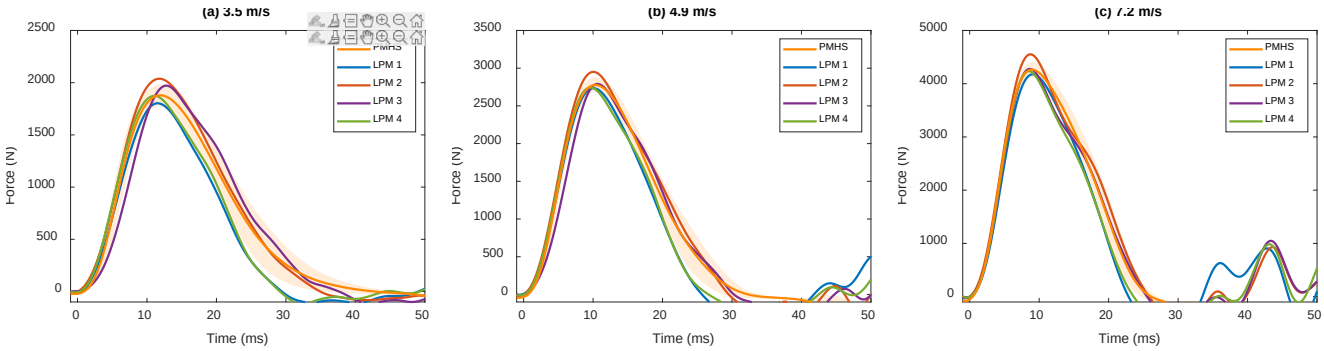

Fig. I5. Average femur force recorded by the left and right femur load cells for all subjects ± SD compared with the individual subject responses predicted by the lumped parameter model for a) 3.5 m/s, b) 4.9 m/s, and c) 7.2 m/s impacts.

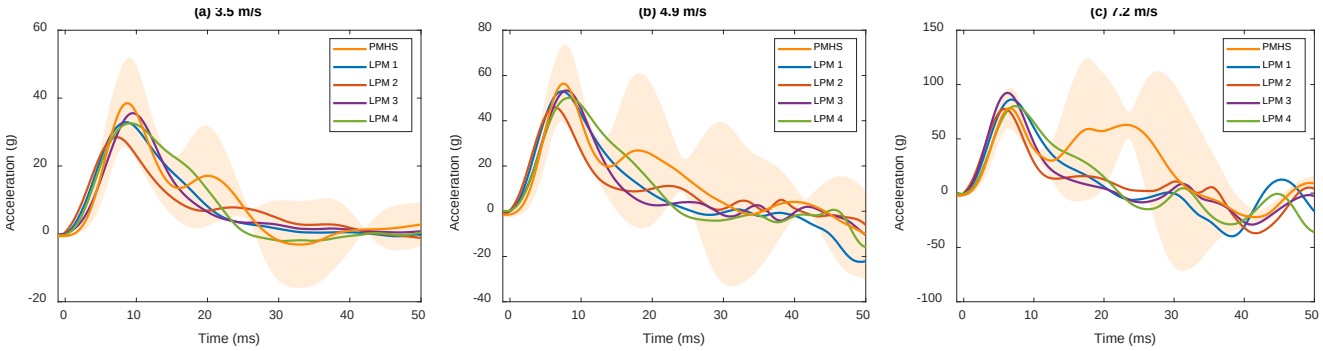

Fig. I6. Average pelvis acceleration for all subjects ± SD compared with the individual subject responses predicted by the lumped parameter model for a) 3.5 m/s, b) 4.9 m/s, and c) 7.2 m/s impacts.

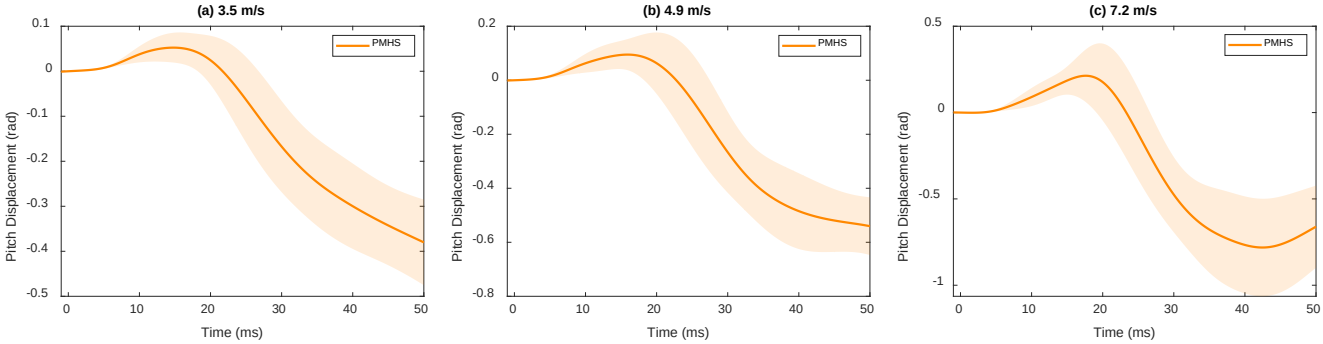

Fig. I7. Average pelvis pitch displacement for all subjects ± SD for a) 3.5 m/s, b) 4.9 m/s, and c) 7.2 m/s impacts.

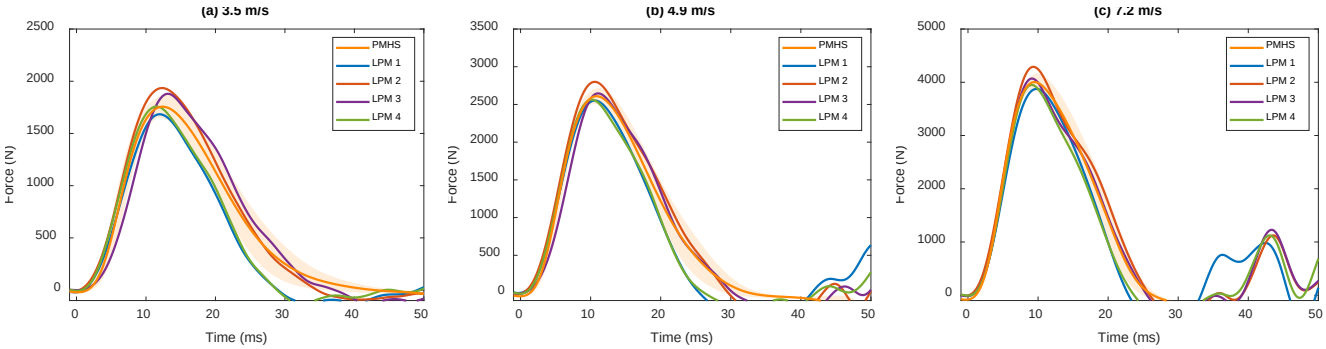

Fig. I8. Average hip force estimated by using an inertial compensation of the left and right femur load cells and the mass between the center of the load cell and the hip for all subjects ± SD compared with the individual subject responses predicted by the lumped parameter model for a) 3.5 m/s, b) 4.9 m/s, and c) 7.2 m/s impacts.

Appendix J: Thigh Flesh Removed Plus Load Cell Condition

TABLE J.I
THIGH FLESH REMOVED PLUS LOAD CELL MODEL

Model Parameter	Subject 1	Subject 2	Subject 3	Subject 4
mA	1.510 kg	1.333 kg	1.611 kg	1.213 kg
mB	0.742 kg	0.626 kg	0.576 kg	0.650 kg
mC	4.527 kg	6.725 kg	5.916 kg	4.815 kg
mD	1.879 kg	2.218 kg	2.830 kg	1.746 kg
mE	10.659 kg	12.927 kg	10.885 kg	8.618 kg
mF	--	--	--	--
mG	0.603 kg	0.624 kg	0.585 kg	0.621 kg
mH	--	--	--	--
kAG	457768 N/m	572456 N/m	441384 N/m	490536 N/m
cAG	2364 Ns/m	4316 Ns/m	5340 Ns/m	1468 Ns/m
kGB	444120 N/m	38616 N/m	661208 N/m	259800 N/m
cGB	1904 Ns/m	3120 Ns/m	976 Ns/m	1040 Ns/m
kBC	141034 N/m	187114 N/m	88810 N/m	3050 N/m
cBC	1184 Ns/m	1080 Ns/m	1064 Ns/m	2616 Ns/m
kAD	15 N/m	15 N/m	15 N/m	11 N/m
cAD	195 Ns/m	220 Ns/m	204 Ns/m	236 Ns/m
kBE	7 N/m	7 N/m	7 N/m	15 N/m
cBE	203 Ns/m	155 Ns/m	34 Ns/m	29 Ns/m
kAF	--	--	--	--
cAF	--	--	--	--
kGH	--	--	--	--
cGH	--	--	--	--

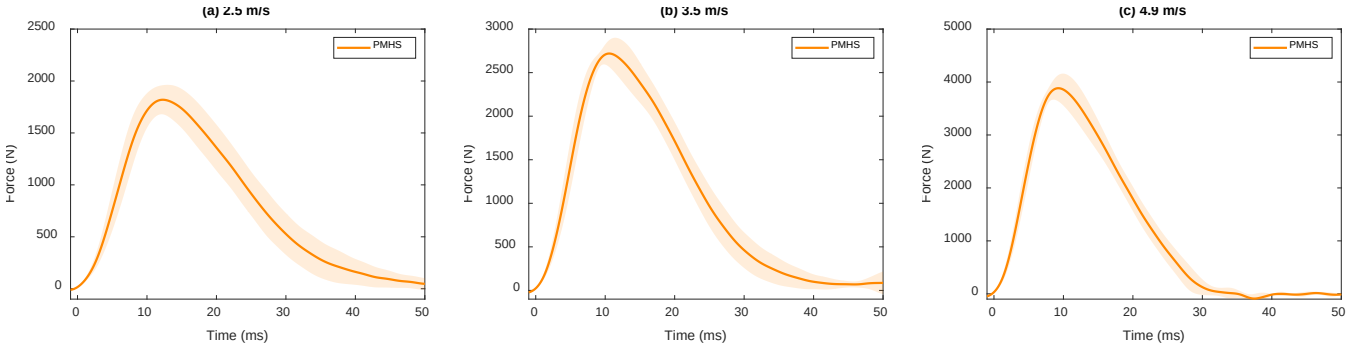

Fig. J1. Average Knee force recorded by the left and right impactor load cells for all subjects ± SD for a) 2.5 m/s, b) 3.5 m/s, and c) 4.9 m/s impacts.

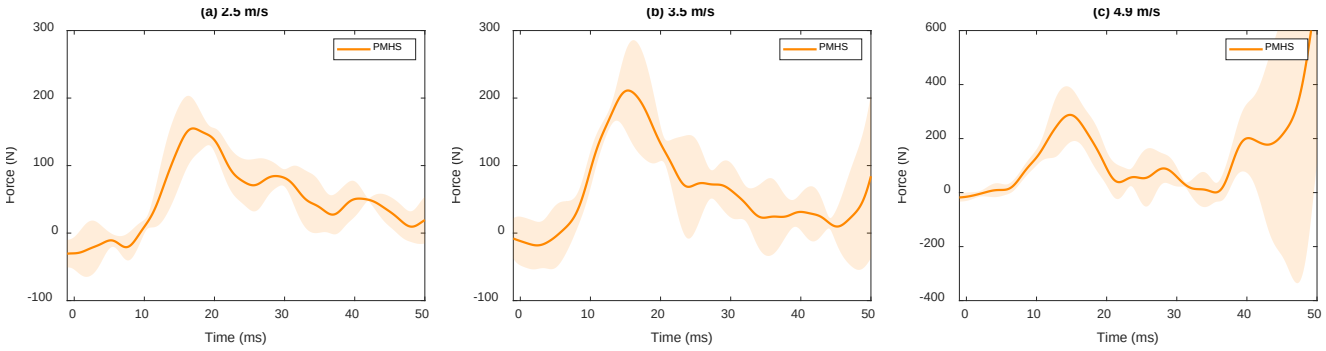

Fig. J2. Average seat friction force for all subjects ± SD for a) 2.5 m/s, b) 3.5 m/s, and c) 4.9 m/s impacts.

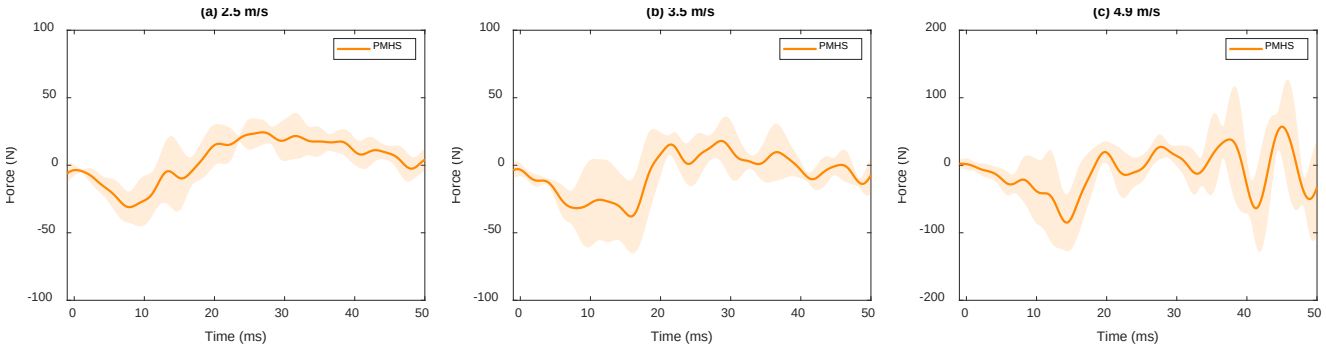

Fig. J3. Average foot friction force for all subjects ± SD for a) 2.5 m/s, b) 3.5 m/s, and c) 4.9 m/s impacts.

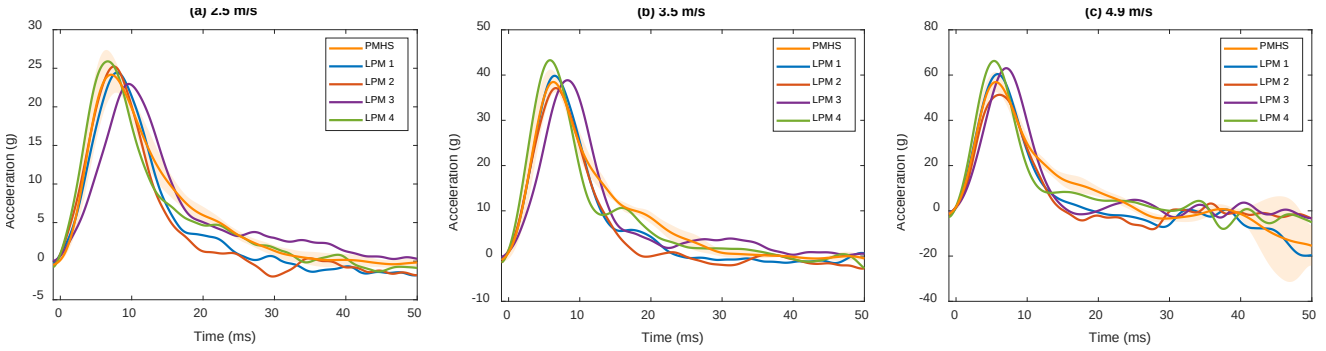

Fig. J4. Average femur acceleration for all subjects ± SD compared with the individual subject responses predicted by the lumped parameter model for a) 2.5 m/s, b) 3.5 m/s, and c) 4.9 m/s impacts.

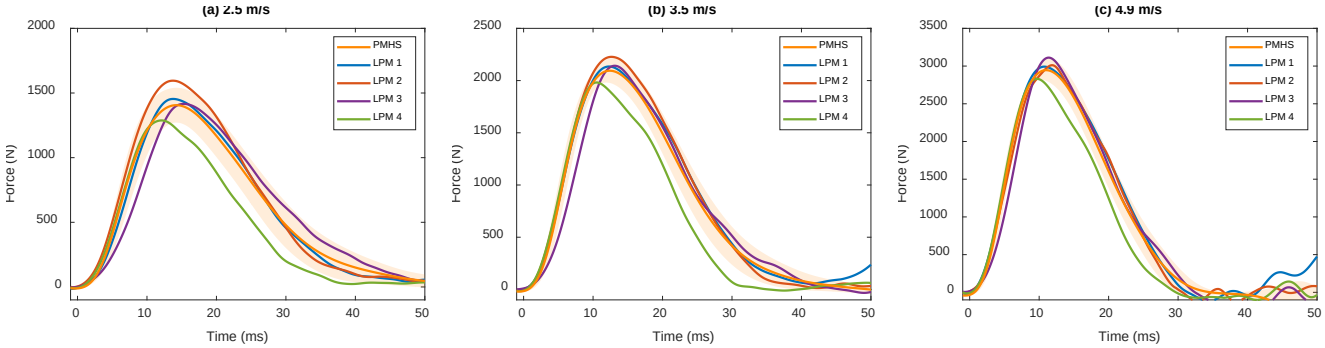

Fig. J5. Average femur force recorded by the left and right femur load cells for all subjects ± SD compared with the individual subject responses predicted by the lumped parameter model for a) 2.5 m/s, b) 3.5 m/s, and c) 4.9 m/s impacts.

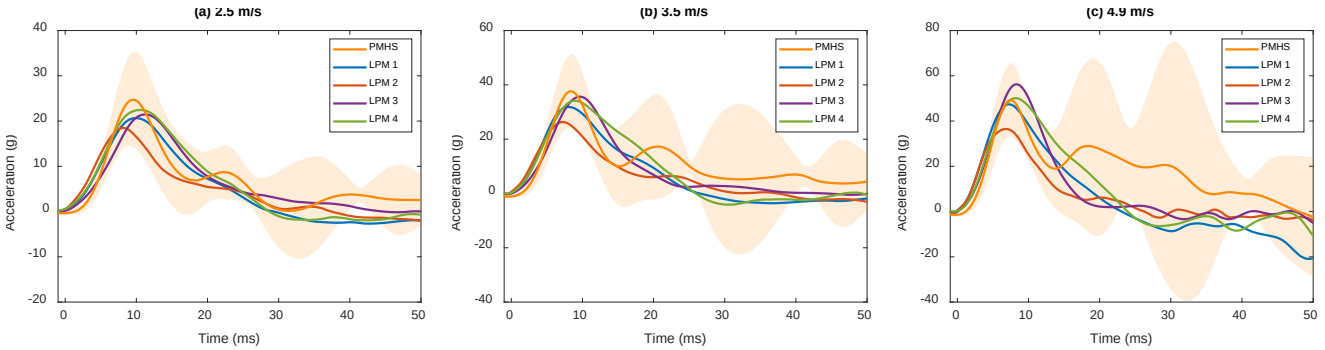

Fig. J6. Average pelvis acceleration for all subjects ± SD compared with the individual subject responses predicted by the lumped parameter model for a) 2.5 m/s, b) 3.5 m/s, and c) 4.9 m/s impacts.

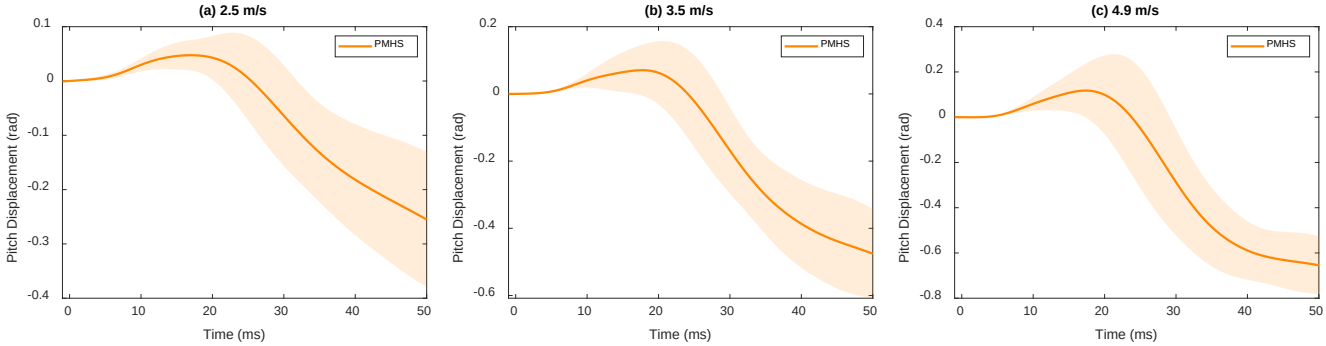

Fig. J7. Average pelvis pitch displacement for all subjects ± SD for a) 2.5 m/s, b) 3.5 m/s, and c) 4.9 m/s impacts.

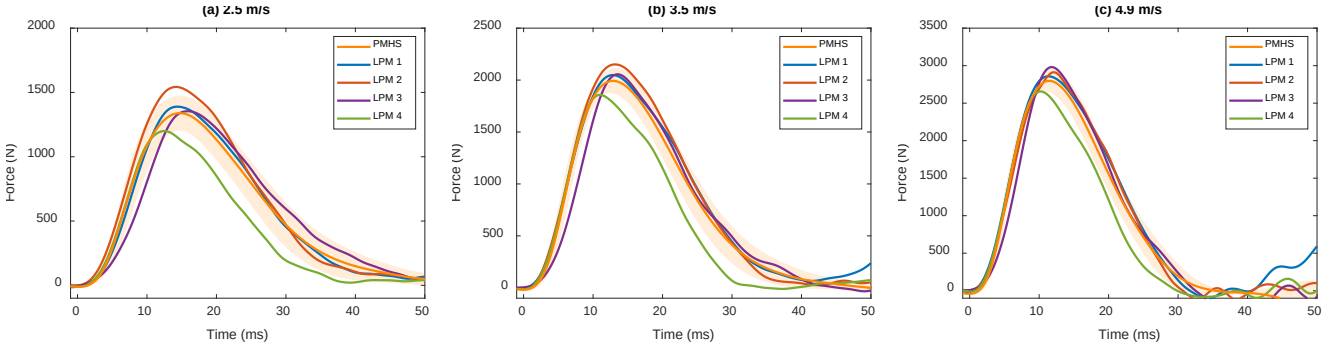

Fig. J8. Average hip force estimated by using an inertial compensation of the left and right femur load cells and the mass between the center of the load cell and the hip for all subjects ± SD compared with the individual subject responses predicted by the lumped parameter model for a) 2.5 m/s, b) 3.5 m/s, and c) 4.9 m/s impacts.

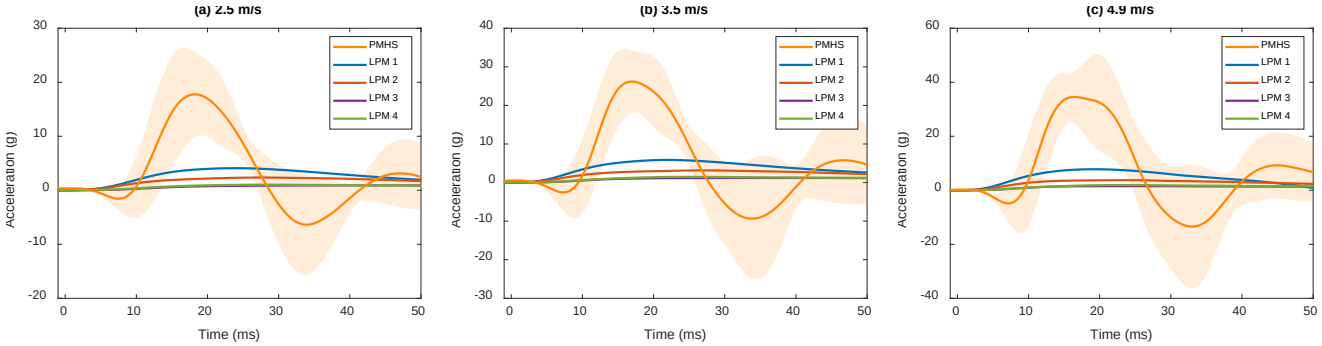

Fig. J9. Average torso (L2) acceleration for all subjects ± SD compared with the individual subject responses predicted by the lumped parameter model for a) 2.5 m/s, b) 3.5 m/s, and c) 4.9 m/s impacts.

Appendix K: Thigh Flesh Removed Condition

TABLE K.I
THIGH FLESH REMOVED MODEL

Model Parameter	Subject 1	Subject 2	Subject 3	Subject 4
mA	1.180 kg	1.009 kg	1.288 kg	0.886 kg
mB	0.742 kg	0.626 kg	0.576 kg	0.650 kg
mC	4.527 kg	6.725 kg	5.916 kg	4.815 kg
mD	1.879 kg	2.218 kg	2.830 kg	1.746 kg
mE	10.659 kg	12.927 kg	10.885 kg	8.618 kg
mF	1.121 kg	1.745 kg	1.486 kg	0.846 kg
mG	0.273 kg	0.301 kg	0.263 kg	0.294 kg
mH	1.121 kg	1.745 kg	1.486 kg	0.846 kg
kAG	457768 N/m	572456 N/m	441384 N/m	490536 N/m
cAG	2364 Ns/m	4316 Ns/m	5340 Ns/m	1468 Ns/m
kGB	444120 N/m	38616 N/m	661208 N/m	259800 N/m
cGB	1904 Ns/m	3120 Ns/m	976 Ns/m	1040 Ns/m
kBC	141034 N/m	187114 N/m	88810 N/m	3050 N/m
cBC	1184 Ns/m	1080 Ns/m	1064 Ns/m	2616 Ns/m
kAD	15 N/m	15 N/m	15 N/m	11 N/m
cAD	195 Ns/m	220 Ns/m	204 Ns/m	236 Ns/m
kBE	7 N/m	7 N/m	7 N/m	15 N/m
cBE	203 Ns/m	155 Ns/m	34 Ns/m	29 Ns/m
kAF	--	--	--	--
cAF	--	--	--	--
kGH	--	--	--	--
cGH	--	--	--	--

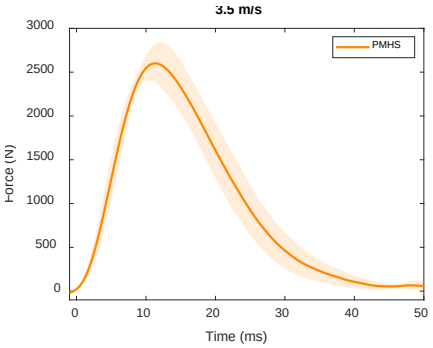

Fig. K1. Average knee force recorded by the left and right impactor load cells for all subjects ± SD for 3.5 m/s impacts.

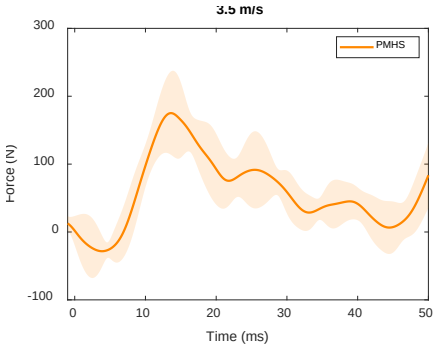

Fig. K2. Average seat friction force for all subjects ± SD for 3.5 m/s impacts.

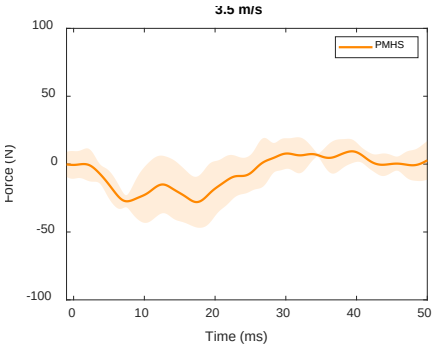

Fig. K3. Average foot friction force for all subjects ± SD for 3.5 m/s impacts.

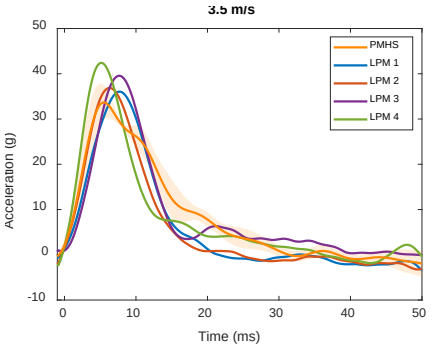

Fig. K4. Average femur acceleration for all subjects ± SD compared with the individual subject responses predicted by the lumped parameter model for 3.5 m/s impacts.

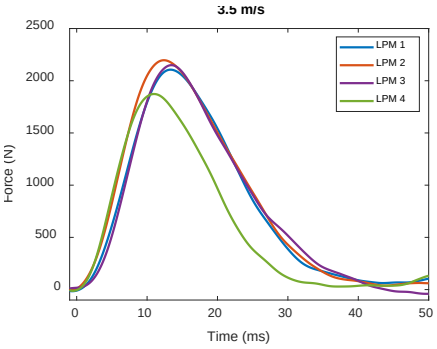

Fig. K5. Femur force individual subject responses predicted by the lumped parameter model for 3.5 m/s impacts.

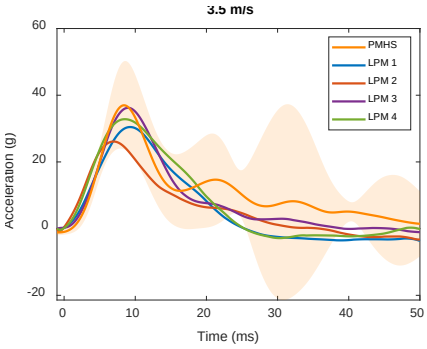

Fig. K6. Average pelvis acceleration for all subjects ± SD compared with the individual subject responses predicted by the lumped parameter model for 3.5 m/s impacts.

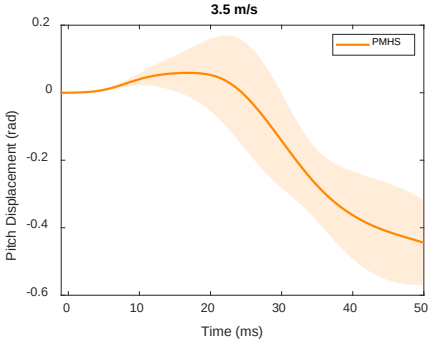

Fig. K7. Average pelvis pitch displacement for all subjects ± SD 3.5 m/s impacts.

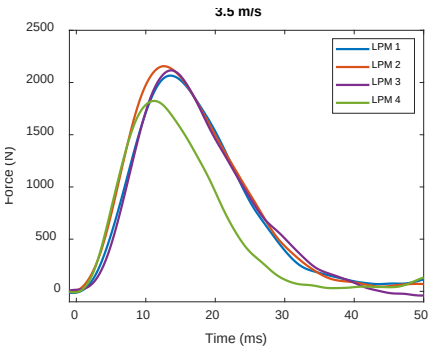

Fig. K8. Hip force individual subject responses predicted by the lumped parameter model for 3.5 m/s impacts.

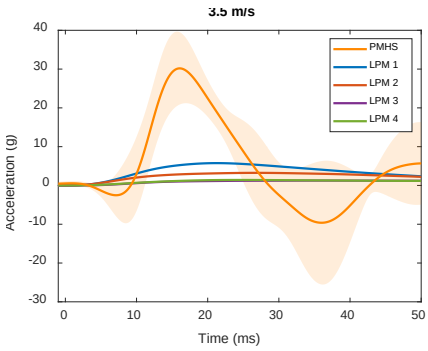

Fig. K9. Average torso (L2) acceleration for all subjects ± SD compared with subject responses predicted by the lumped parameter model for 3.5 m/s impacts.

Appendix L: Whole Body Condition

TABLE L.I
WHOLE BODY MODEL

Model Parameter	Subject 1	Subject 2	Subject 3	Subject 4
mA	1.180 kg	1.009 kg	1.288 kg	0.886 kg
mB	0.742 kg	0.626 kg	0.576 kg	0.650 kg
mC	4.527 kg	6.725 kg	5.916 kg	4.815 kg
mD	1.879 kg	2.218 kg	2.830 kg	1.746 kg
mE	10.659 kg	12.927 kg	10.885 kg	8.618 kg
mF	1.121 kg	1.745 kg	1.486 kg	0.846 kg
mG	0.273 kg	0.301 kg	0.263 kg	0.294 kg
mH	1.121 kg	1.745 kg	1.486 kg	0.846 kg
kAG	457768 N/m	572456 N/m	441384 N/m	490536 N/m
cAG	2364 Ns/m	4316 Ns/m	5340 Ns/m	1468 Ns/m
kGB	444120 N/m	38616 N/m	661208 N/m	259800 N/m
cGB	1904 Ns/m	3120 Ns/m	976 Ns/m	1040 Ns/m
kBC	141034 N/m	187114 N/m	88810 N/m	3050 N/m
cBC	1184 Ns/m	1080 Ns/m	1064 Ns/m	2616 Ns/m
kAD	15 N/m	15 N/m	15 N/m	11 N/m
cAD	195 Ns/m	220 Ns/m	204 Ns/m	236 Ns/m
kBE	7 N/m	7 N/m	7 N/m	15 N/m
cBE	203 Ns/m	155 Ns/m	34 Ns/m	29 Ns/m
kAF	62654 N/m	101566 N/m	48318 N/m	59582 N/m
cAF	116 Ns/m	212 Ns/m	148 Ns/m	108 Ns/m
kGH	62654 N/m	101566 N/m	48318 N/m	59582 N/m
cGH	116 Ns/m	212 Ns/m	148 Ns/m	108 Ns/m

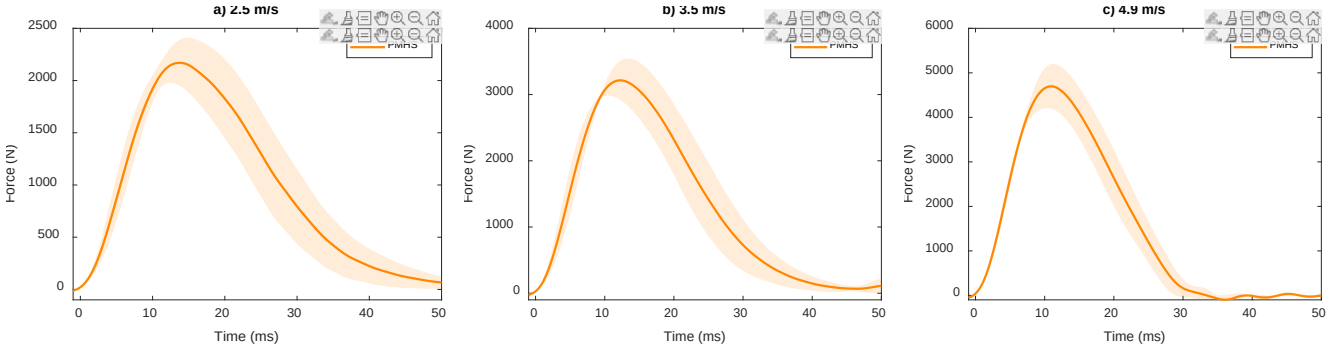

Fig. L1. Average Knee force recorded by the left and right impactor load cells for all subjects ± SD for a) 2.5 m/s, b) 3.5 m/s, and c) 4.9 m/s impacts.

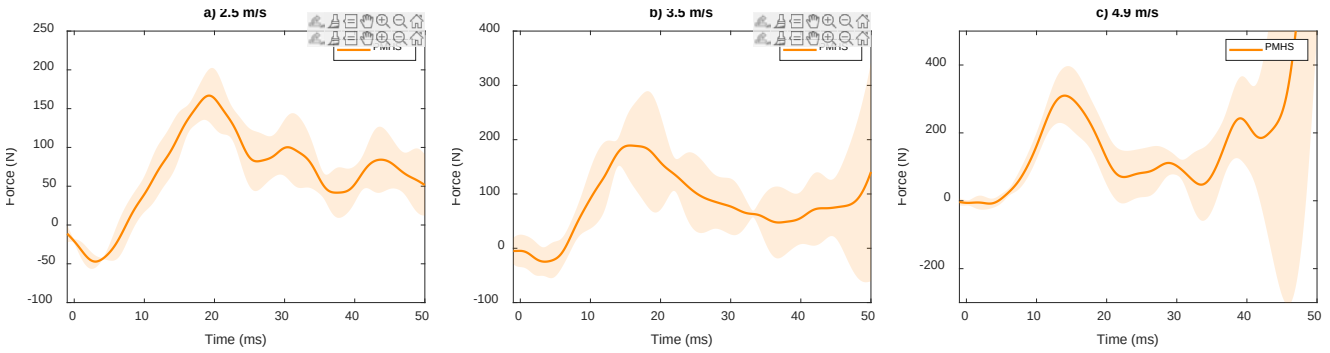

Fig. L2. Average seat friction force for all subjects ± SD for a) 2.5 m/s, b) 3.5 m/s, and c) 4.9 m/s impacts.

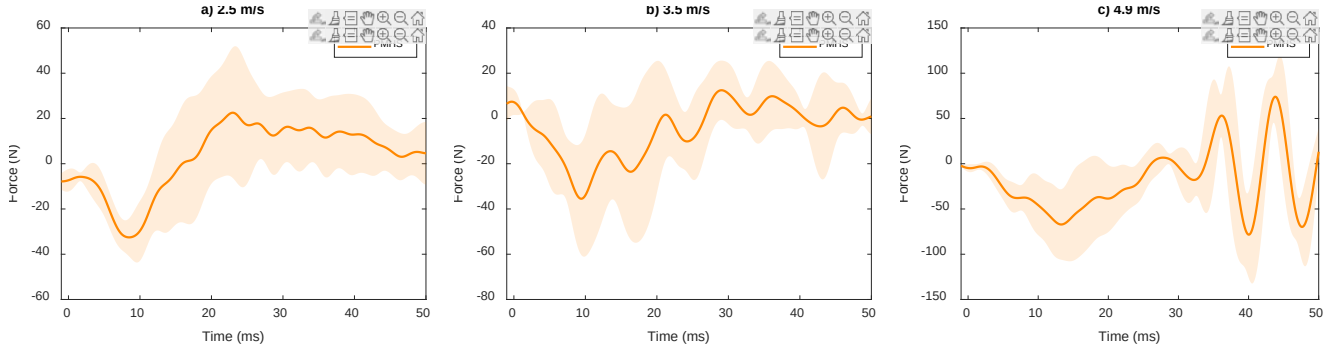

Fig. L3. Average foot friction force for all subjects ± SD for a) 2.5 m/s, b) 3.5 m/s, and c) 4.9 m/s impacts.

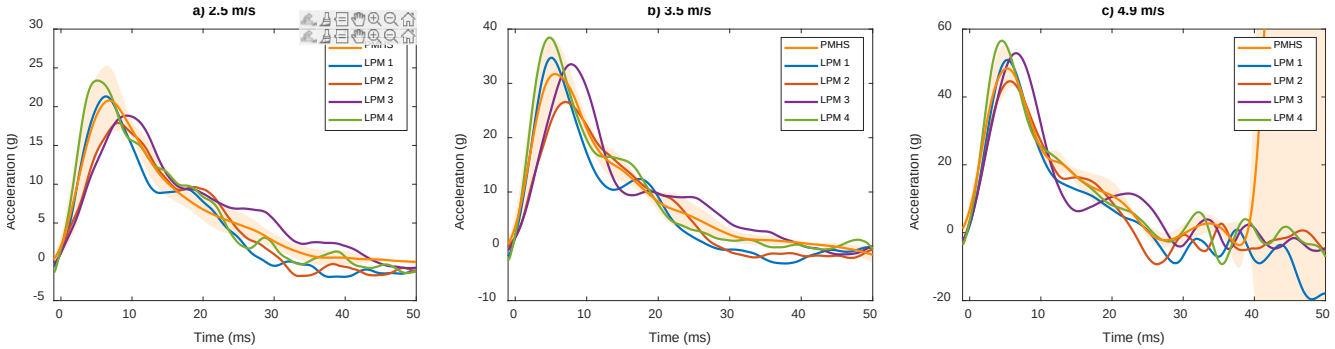

Fig. L4. Average femur acceleration for all subjects ± SD compared with the individual subject responses predicted by the lumped parameter model for a) 2.5 m/s, b) 3.5 m/s, and c) 4.9 m/s impacts.

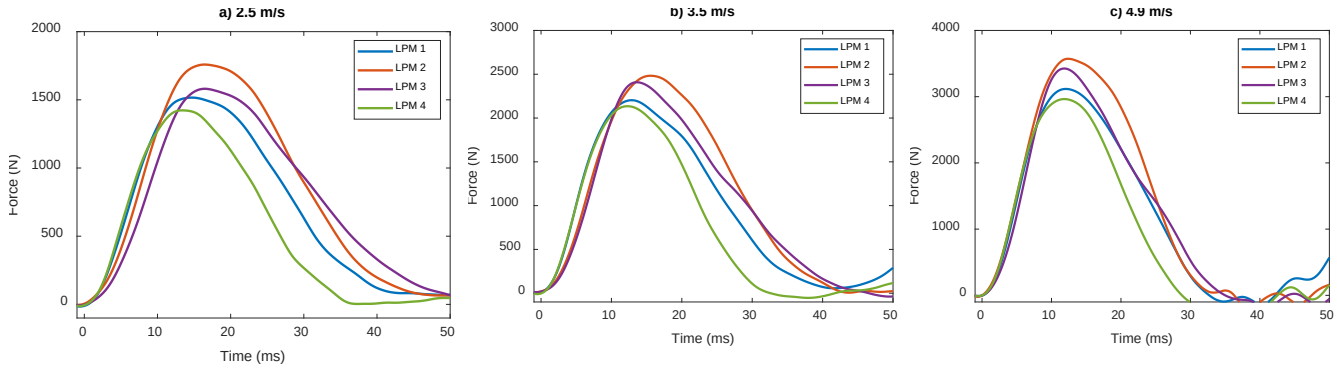

Fig. L5. Femur force individual subject responses predicted by the lumped parameter model for a) 2.5 m/s, b) 3.5 m/s, and c) 4.9 m/s impacts.

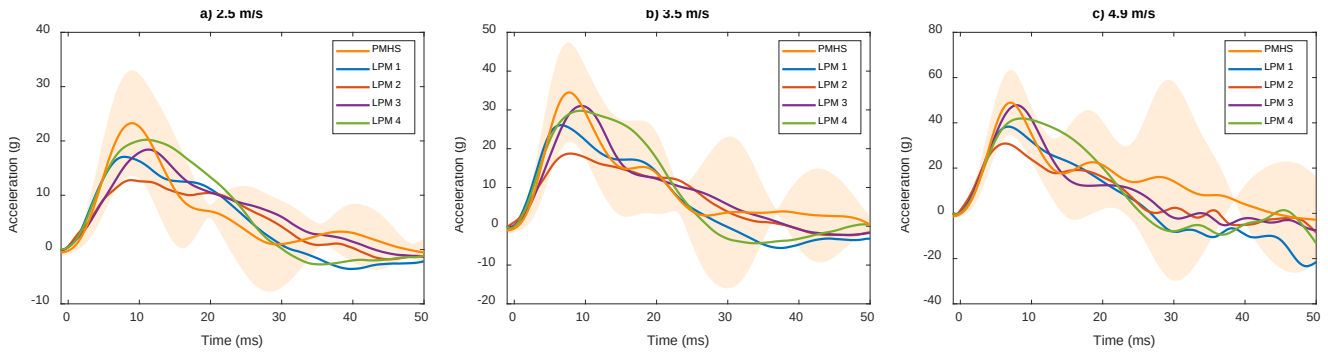

Fig. L6. Average pelvis acceleration for all subjects ± SD compared with the individual subject responses predicted by the lumped parameter model for a) 2.5 m/s, b) 3.5 m/s, and c) 4.9 m/s impacts.

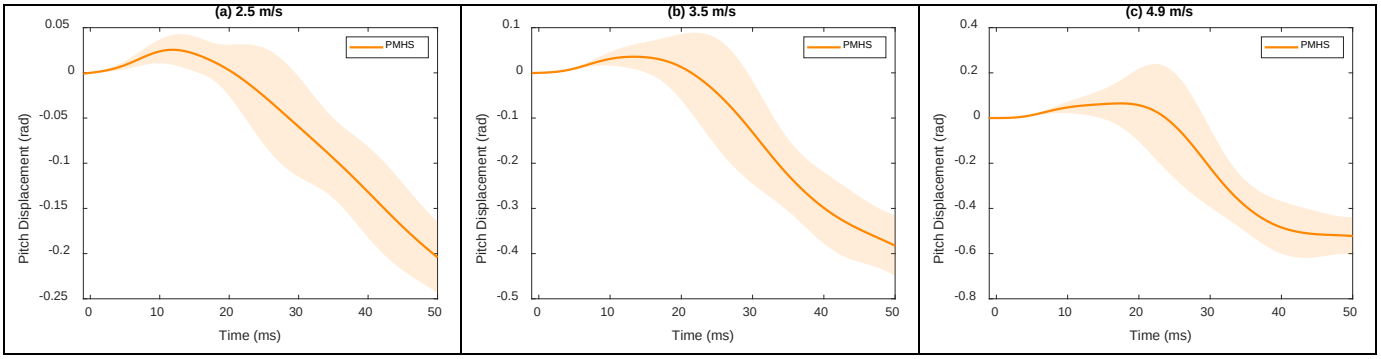

Fig. L7. Average pelvis pitch displacement for all subjects ± SD for a) 2.5 m/s, b) 3.5 m/s, and c) 4.9 m/s impacts.

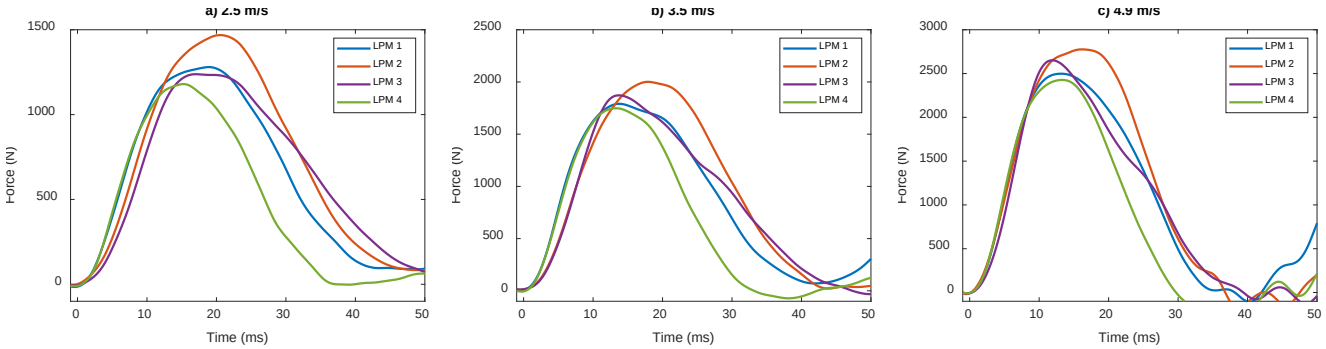

Fig. L7. Hip force individual subject responses predicted by the lumped parameter model for a) 2.5 m/s, b) 3.5 m/s, and c) 4.9 m/s impacts.

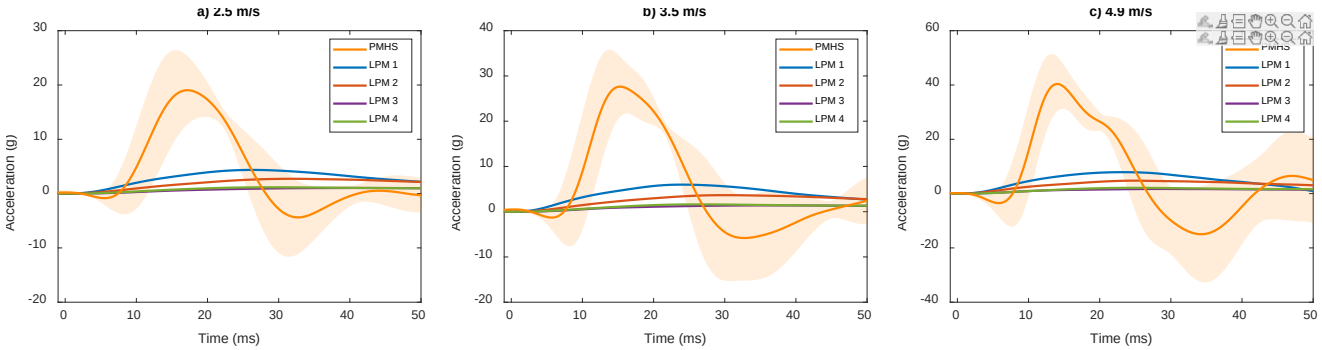

Fig. L8. Average torso (L2) acceleration for all subjects ± SD compared with the individual subject responses predicted by the lumped parameter model for a) 2.5 m/s, b) 3.5 m/s, and c) 4.9 m/s impacts.

Appendix M: Femur Loading Characteristics

TABLE M.I
FEMUR LOADING CHARACTERISTICS FOR 2.5 M/S IMPACTS

Subject Condition	Subject	Loading Rate (N/ms)	Loading Duration (ms)	Time to Peak Force (ms)	Maximum force (kN)
WB	1	165	34.0	14.7	1.52
	2	171	34.4	16.4	1.76
	3	152	38.1	16.5	1.58
	4	164	28.3	13.4	1.42
	Average (±SD)	163 (±8)	33.7 (±4.0)	15.3 (±1.5)	1.57 (±0.14)
TFR+LC	1	170	31.3	13.8	1.45
	2	184	30.1	13.7	1.60
	3	144	35.7	15.3	1.42
	4	173	26.9	12.1	1.29
	Average (±SD)	168 (±17)	31.0 (±3.6)	13.7 (±1.3)	1.44 (±0.13)

TABLE M.II
FEMUR LOADING CHARACTERISTICS FOR 3.5 M/S IMPACTS

Subject Condition	Subject	Loading Rate (N/ms)	Loading Duration (ms)	Time to Peak Force (ms)	Maximum force (kN)
WB	1	279	30.4	12.9	2.20
	2	255	31.7	15.6	2.48
	3	272	33	13.6	2.41
	4	273	25.2	12.3	2.13
	Average (±SD)	270 (±10)	30.1 (±3.4)	13.6 (±1.4)	2.31 (±0.16)
TFR	1	239	27.5	13.3	2.11
	2	273	28.8	12.4	2.20
	3	260	28.9	13.5	2.15
	4	266	24.2	11.0	1.87
	Average (±SD)	260 (±15)	27.4 (±2.2)	12.6 (±1.1)	2.08 (±0.14)
TFR+LC	1	280	28.4	12.3	2.13
	2	285	28.1	12.6	2.23
	3	261	28.9	13.1	2.14
	4	290	24.2	10.5	1.98
	Average (±SD)	279 (±13)	27.4 (±2.2)	12.1 (±1.1)	2.12 (±0.10)
ToR	1	239	22.3	11.5	1.80
	2	272	25.9	11.8	2.04
	3	251	26.3	12.8	1.97
	4	263	22.4	11.1	1.87
	Average (±SD)	256 (±14)	24.2 (±2.2)	11.8 (±0.7)	1.92 (±0.10)

TABLE M.III
FEMUR LOADING CHARACTERISTICS FOR 4.9 M/S IMPACTS

Subject Condition	Subject	Loading Rate (N/ms)	Loading Duration (ms)	Time to Peak Force (ms)	Maximum force (kN)
WB	1	421	26.4	12.1	3.12
	2	436	26.0	12.4	3.57
	3	450	27.0	11.8	3.43
	4	420	23.3	11.8	2.96
	Average (±SD)	432 (±14)	25.7 (±1.6)	12.0 (±0.3)	3.27 (±0.28)
TFR+LC	1	449	24.6	10.7	2.99
	2	410	24.0	11.9	3.01
	3	434	24.8	11.4	3.11
	4	461	21.8	9.7	2.83
	Average (±SD)	439 (±22)	23.8 (±1.4)	10.9 (±1.0)	2.99 (±0.12)
ToR	1	424	20.3	10.0	2.73
	2	449	23.7	10.0	2.95
	3	406	23.3	10.6	2.79
	4	441	20.3	9.6	2.74
	Average (±SD)	430 (±19)	21.9 (±1.9)	10.1 (±0.4)	2.80 (±0.10)

TABLE M.IV
FEMUR LOADING CHARACTERISTICS FOR 7.2 M/S IMPACTS

Subject Condition	Subject	Loading Rate (N/ms)	Loading Duration (ms)	Time to Peak Force (ms)	Maximum force (kN)
ToR	1	729	18.7	9.1	4.18
	2	792	20.8	8.7	4.55
	3	765	20.5	8.7	4.28
	4	779	19.0	8.5	4.24
	Average (±SD)	766 (±27)	19.8 (±1.1)	8.8 (±0.3)	4.31 (±0.17)

Appendix N: Hip Loading Characteristics

TABLE N.I
HIP LOADING CHARACTERISTICS FOR 2.5 M/S IMPACTS

Subject Condition	Subject	Loading Rate (N/ms)	Loading Duration (ms)	Time to Peak Force (ms)	Maximum force (kN)
WB	1	125	35.2	18.9	1.28
	2	123	36.2	20.5	1.47
	3	119	39.7	17.1	1.24
	4	125	29.0	15.2	1.18
	Average (±SD)	123 (±3)	35.0 (±4.5)	17.9 (±2.3)	1.29 (±0.12)
TFR+LC	1	162	31.2	14.4	1.39
	2	175	29.8	14.2	1.54
	3	140	35.1	15.9	1.35
	4	167	26.5	12.5	1.20
	Average (±SD)	161 (±15)	30.7 (±3.6)	14.3 (±1.4)	1.37 (±0.14)

TABLE N.II
HIP LOADING CHARACTERISTICS FOR 3.5 M/S IMPACTS

Subject Condition	Subject	Loading Rate (N/ms)	Loading Duration (ms)	Time to Peak Force (ms)	Maximum force (kN)
WB	1	215	32.6	13.8	1.79
	2	177	33.5	17.9	2.00
	3	212	34.9	13.7	1.87
	4	213	26.0	13.3	1.75
	Average (±SD)	204 (±18)	31.8 (±3.9)	14.7 (±2.2)	1.85 (±0.11)
TFR	1	234	27.5	13.5	2.07
	2	270	28.6	12.6	2.16
	3	258	28.6	13.6	2.12
	4	261	23.9	11.2	1.82
	Average (±SD)	255 (±15)	27.2 (±2.2)	12.7 (±1.1)	2.04 (±0.15)
TFR+LC	1	262	28.3	12.8	2.05
	2	270	27.9	13.2	2.15
	3	253	28.1	13.5	2.06
	4	276	23.8	11.0	1.86
	Average (±SD)	265 (±10)	27.0 (±2.2)	12.6 (±1.1)	2.03 (±0.12)
ToR	1	221	21.7	12.0	1.68
	2	258	25.3	12.3	1.93
	3	241	25.6	13.2	1.88
	4	247	21.8	11.5	1.76
	Average (±SD)	242 (±16)	23.6 (±2.1)	12.3 (±0.7)	1.81 (±0.11)

TABLE N.III
HIP LOADING CHARACTERISTICS FOR 4.9 M/S IMPACTS

Subject Condition	Subject	Loading Rate (N/ms)	Loading Duration (ms)	Time to Peak Force (ms)	Maximum force (kN)
WB	1	332	28.2	13.1	2.50
	2	305	28.7	16.1	2.78
	3	355	29.0	11.9	2.65
	4	331	24.2	13.3	2.43
	Average (±SD)	331 (±20)	27.5 (±2.2)	13.6 (±1.8)	2.59 (±0.16)
TFR+LC	1	420	24.5	11.3	2.86
	2	390	23.9	12.1	2.91
	3	421	24.3	11.8	2.98
	4	431	21.3	10.2	2.66
	Average (±SD)	415 (±18)	23.5 (±1.5)	11.4 (±0.8)	2.85 (±0.14)
ToR	1	388	19.8	10.6	2.55
	2	418	23.4	10.6	2.80
	3	392	22.6	11.1	2.65
	4	412	19.7	10.2	2.56
	Average (±SD)	402 (±15)	21.4 (±1.9)	10.6 (±0.4)	2.64 (±0.11)

TABLE N.IV
HIP LOADING CHARACTERISTICS FOR 7.2 M/S IMPACTS

Subject Condition	Subject	Loading Rate (N/ms)	Loading Duration (ms)	Time to Peak Force (ms)	Maximum force (kN)
ToR	1	657	18.3	9.8	3.87
	2	723	20.7	9.3	4.29
	3	732	20.1	9.1	4.07
	4	719	18.4	9.1	3.95
	Average (±SD)	708 (±35)	19.4 (±1.2)	9.3 (±0.3)	4.05 (±0.18)

Appendix O: Force Transfer

TABLE O.I
WHOLE BODY FORCE TRANSFER

Impact Velocity (m/s)	Subject	Femur Force Transfer (%)	Hip Force Transfer (%)
2.5	1	72.1	60.9
	2	72.2	60.2
	3	69.0	54.0
	4	72.0	59.7
	Average (± SD)	71.3 (±1.6)	58.7 (±3.2)
3.5	1	71.36	57.99
	2	71.47	57.61
	3	68.36	53.14
	4	72.24	59.16
	Average (± SD)	70.9 (±1.7)	57.0 (±2.6)
4.9	1	70.24	56.29
	2	69.37	53.91
	3	67.20	52.02
	4	71.58	58.62
	Average (± SD)	69.6 (±1.8)	55.2 (±2.9)
WB Average (± SD)		70.6 (±1.7)	57.0 (±3.0)

TABLE O.II
THIGH FLESH REMOVED FORCE TRANSFER

Impact Velocity (m/s)	Subject	Femur Force Transfer (%)	Hip Force Transfer (%)
3.5	1	79.6	78.1
	2	80.7	79.3
	3	77.2	76.0
	4	79.3	77.2
	Average (± SD)	79.2 (±1.5)	77.7 (±1.4)

TABLE O.III
THIGH FLESH REMOVED + LOAD CELL FORCE TRANSFER

Impact Velocity (m/s)	Subject	Femur Force Transfer (%)	Hip Force Transfer (%)
2.5	1	77.9	74.5
	2	80.6	78.0
	3	75.3	72.0
	4	77.1	71.8
	Average (± SD)	77.7 (±2.2)	74.2 (±2.9)
3.5	1	77.1	74.0
	2	79.6	76.9
	3	74.4	71.4
	4	77.2	72.3
	Average (± SD)	77.1 (±2.1)	73.7 (±2.4)
4.9	1	75.5	72.1
	2	79.9	77.3
	3	73.4	70.3
	4	76.4	71.7
	Average (± SD)	76.3 (±2.7)	72.8 (±3.1)
TFR+LC Average (± SD)		77.0 (±2.2)	73.5 (±2.6)

TABLE O.IV
TORSO REMOVED FORCE TRANSFER

Impact Velocity (m/s)	Subject	Femur Force Transfer (%)	Hip Force Transfer (%)
2.5	1	72.7	67.9
	2	75.8	71.9
	3	73.2	69.8
	4	76.9	72.2
	Average (± SD)	74.6 (±2.0)	70.5 (±2.0)
3.5	1	71.5	66.7
	2	74.7	70.9
	3	71.9	68.1
	4	75.5	70.5
	Average (± SD)	73.4 (±2.0)	69.1 (±2.0)
4.9	1	68.9	63.9
	2	72.5	68.3
	3	70.1	66.7
	4	74.1	69.1
	Average (± SD)	71.4 (±2.3)	67.0 (±2.3)
ToR Average (± SD)		73.1 (±2.4)	68.8 (±2.4)

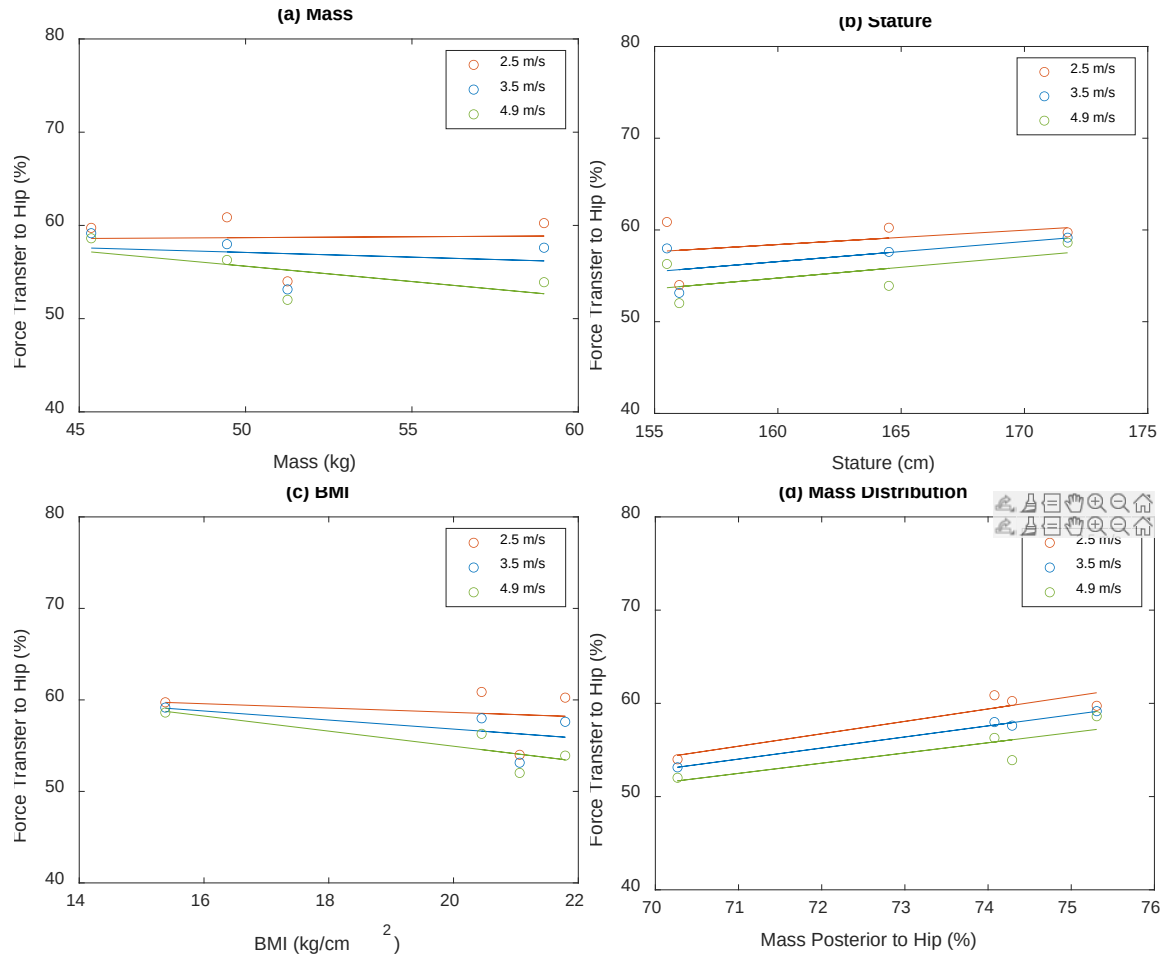

Fig. O1. LPM predicted force transfer to the hip for each subject at each impact velocity as a function of a) subject mass, b) subject stature, c) subject BMI, and d) subject mass distribution (represented by the mass posterior to the hip divided by the total subject mass).